and heart failure.

### 4. MRTF-A is a novel transcriptional mediator linking actin remodeling and cardiac gene expression

Hemodynamic overload caused by a combination of mechanical stress and neurohumoral stimulation induces a hypertrophic response characterized in part by reactivation of the fetal gene program in cardiac myocytes (1, 24). Among the variety of intracellular signaling molecules known to be activated following mechanical stretch or neurohumoral stimulation, Rho family small GTPases, especially Rho A and Rac1, have been highlighted as important regulators for cardiac hypertrophy (25, 26).

A transcriptional activator, serum response factor (SRF), has been shown to be involved in the downstream mechanisms by which Rho GTPases activate the hypertrophic gene program. SRF is a MADS-box transcription factor that regulates the expression of immediate early genes and muscle-specific genes by binding to a conserved sequence [CC (A/T) $_6$GG] known as the CArG box or serum response element. In this way, SRF plays an important role in the induction of a subset of cardiac genes during adverse cardiac remodeling. Targeted deletion of SRF in the developing heart results in lethal cardiac defects with reduced expression of many cardiac-specific genes (27, 28). In addition, overexpression of SRF in the postnatal heart leads to cardiomyopathy with increased fetal cardiac gene expression (29), while conditional deletion of SRF in isolated neonatal cardiac myocytes results in reduced expression of hypertrophic genes (30). Indeed, several fetal cardiac genes, including ANP, skeletal $\alpha$-actin, smooth muscle $\alpha$-actin, and smooth muscle 22$\alpha$, contain a functionally important CArG box in their upstream transcription control regions (31, 32). At least two signaling pathways are known to modulate SRF activity: one involving the phosphorylation of ternary complex factors in Ets-domain family proteins and another controlled by Rho-family small GTPases and actin dynamics (33, 34). It was recently shown in NIH3T3 cells that stimulation of Rho- and actin dynamics–dependent signaling results in translocation of a novel SRF co-factor, myocardin-related transcription factor (MRTF)-A (also known as MAL or MKL1), from G-actin in the cytoplasm to the nucleus, leading to activation of SRF target genes (35, 36).

We further showed that Rho- and actin treadmill–dependent nuclear accumulation of MRTF-A contributes to the transduction of mechanical stress to SRF-dependent transcriptional activation of fetal cardiac genes in cardiac myocytes. In mice lacking MRTF-A, induction of BNP and other fetal cardiac genes in response to both acute and chronic pressure overload was significantly attenuated. We also revealed the involvement of MRTF-A in chronic cardiac remodeling, a process in which neurohumoral factors play a pivotal role. Following stimulation with angiotensin II or endothelin-1, MRTF-A was translocated into the nuclei of cardiac myocytes, where it activated SRF. Moreover, MRTF-A$^{-/-}$ mice showed significantly weaker hypertrophic responses than their wild-type littermates. Collectively, these findings indicate that MRTF-A is a common mediator of mechanical stress– and neurohumoral stimulation–induced prohypertrophic signaling (Fig. 3) (37).

The inhibition of Rho or ROCK (Rho kinase), a downstream target of Rho, ameliorates pathological cardiac hypertrophy (25, 38, 39). Our study defines MRTF-A as a critical downstream mediator of Rho- and actin dynamics–associated prohypertrophic signaling in cardiac myocytes, while others have shown that in epithelial cells MRTF-A is also activated downstream of Rac (40). Two important events that occur downstream of Rho and Rac activation are alteration of actin cytoskeletal organization and gene transcription, and MRTF-A is a key mediator of the latter. Consequently, diminishing MRTF-A–mediated transcriptional activation by inhibiting its nuclear translocation and/or its co-activator function, which would selectively block transcriptional pathways activated downstream of Rho family small GTPases, could be a safer and more specific therapeutic approach to preventing pathological cardiac remodeling, without the potential side effects caused by disruption of the physiological organization of the actin-cytoskeleton (Fig. 3).

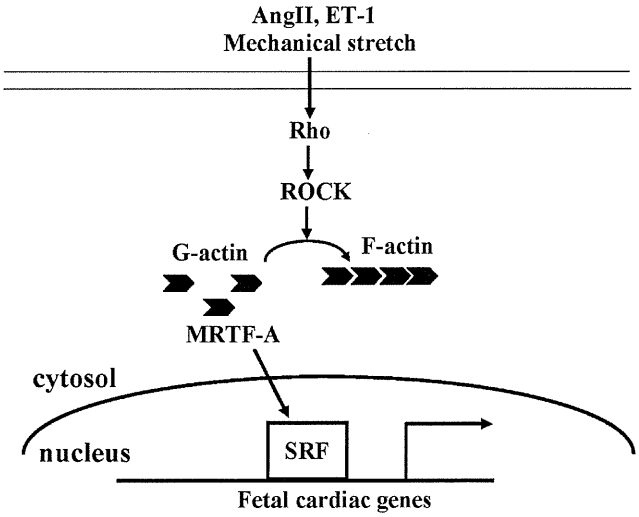


**Fig. 3.** Nuclear translocation of MRTF-A following Rho–ROCK activation and actin remodeling mediates both mechanical stress– and neurohumoral stimulation–inducible hypertrophic gene reprogramming.

## 5. Conclusion

Genetic remodeling contributes to the progression of heart failure by affecting myocardial cellular function and survival. Exploring the transcriptional pathways involved in pathological cardiac remodeling will lead to a better understanding of the molecular mechanisms underlying the development of pathological processes in the heart and will ultimately provide us with an opportunity to shed light on new molecular effectors with the potential to have a therapeutic impact on human heart failure. In this mini-review, we have introduced our work on the transcriptional pathways involved in pathological cardiac remodeling. A transcriptional repressor, NRSF, represses expression of multiple fetal cardiac genes through recruitment of HDACs, and attenuation of this NRSF-mediated repression appears to contribute to the re-expression of fetal cardiac genes in diseased hearts. Inhibition of NRSF in the heart results in cardiac dysfunction and sudden arrhythmic death accompanied by re-expression of multiple fetal genes, including those encoding fetal ion channels, such as the T-type $Ca^{2+}$ channel. Conversely, T-type $Ca^{2+}$-channel blockade significantly prolongs survival in dnNRSF-Tg mice (12). TRPC6 is a key integrated component of the calcineurin–NFAT signaling circuit, and its inhibition significantly ameliorates the pathological process in mouse models of cardiac hypertrophy. This at least in part reflects the fact that inhibition of TRPC6 contributes to the antihypertrophic effects exerted by ANP/BNP – GC-A – PKG signaling, which suggests TRPC6 blockade could be a novel therapeutic strategy for preventing pathological cardiac remodeling. Finally, we revealed a new signaling mechanism whereby MRTF-A, a co-activator of SRF, mediates both mechanical stress– and neurohumoral stimulation–induced prohypertrophic signaling by linking the small GTPase Rho-actin dynamics signaling pathway to cardiac gene transcription. Collectively, our studies on the transcriptional network underlying the pathological cardiac remodeling have revealed several potential therapeutic targets; T-type $Ca^{2+}$ channel, TRPC6 channel, and MRTF-A. We anticipate that further study of the transcriptional network involved in the development of cardiac dysfunction will lead to the discovery of new therapeutic targets for the treatment of heart failure.

## Acknowledgments

We thank Dr. T. Iwamoto (Fukuoka University) for giving us the opportunity to write this review article. We also thank Y. Kubo for her excellent secretarial work. Work carried in our laboratories is supported by Grants-in-Aid for Scientific Research from the Japan Society for the Promotion of Science (to K.K. and N.K.) and grants from the Japanese Ministry of Health, Labour, and Welfare (to N.K.).

## References

1 Olson EN. A decade of discoveries in cardiac biology. Nat Med. 2004;10:467–474.
2 Kraner SD, Chong JA, Tsay HJ, Mandel G. Silencing the type II sodium channel gene: A model for neural-specific gene regulation. Neuron. 1992;9:37–44.
3 Mori N, Schoenherr C, Vandenbergh DJ, Anderson DJ. A common silencer element in the SCG10 and type II Na+ channel genes binds a factor present in nonneuronal cells but not in neuronal cells. Neuron. 1992;9:45–54.
4 Chong JA, Tapia-Ramirez J, Kim S, Toledo-Aral JJ, Zheng Y, Boutros MC, et al. REST: A mammalian silencer protein that restricts sodium channel gene expression to neurons. Cell. 1995; 80:949–957.
5 Schoenherr CJ, Anderson DJ. The neuron-restrictive silencer factor (NRSF): A coordinate repressor of multiple neuron-specific genes. Science. 1995;267:1360–1363.
6 Kuwahara K, Saito Y, Ogawa E, Takahashi N, Nakagawa Y, Naruse Y, et al. The neuron-restrictive silencer element-neuron-restrictive silencer factor system regulates basal and endothelin 1-inducible atrial natriuretic peptide gene expression in ventricular myocytes. Mol Cell Biol. 2001;21:2085–2097.
7 Ogawa E, Saito Y, Kuwahara K, Harada M, Miyamoto Y, Hamanaka I, et al. Fibronectin signaling stimulates BNP gene transcription by inhibiting neuron-restrictive silencer element-dependent repression. Cardiovasc Res. 2002;53:451–459.
8 Kuwahara K, Saito Y, Takano M, Arai Y, Yasuno S, Nakagawa Y, et al. NRSF regulates the fetal cardiac gene program and maintains normal cardiac structure and function. EMBO J. 2003;22: 6310–6321.
9 Nakagawa Y, Kuwahara K, Harada M, Takahashi N, Yasuno S, Adachi Y, et al. Class II HDACS mediate CaMK-dependent signaling to NRSF in ventricular myocytes. J Mol Cell Cardiol. 2006;41:1010–1022.
10 McKinsey TA, Zhang CL, Lu J, Olson EN. Signal-dependent nuclear export of a histone deacetylase regulates muscle differentiation. Nature. 2000;408:106–111.
11 Kinoshita H, Kuwahara K, Takano M, Arai Y, Kuwabara Y, Yasuno S, et al. T-type Ca2+ channel blockade prevents sudden death in mice with heart failure. Circulation. 2009;120:743–752.
12 Furukawa T, Miura R, Honda M, Kamiya N, Mori Y, Takeshita S, et al Identification of R(-)-isomer of efonidipine as a selective blocker of T-type Ca2+ channels. Br J Pharmacol. 2004;143: 1050–1057.
13 Molkentin JD, Lu JR, Antos CL, Markham B, Richardson J, Robbins J, et al. A calcineurin-dependent transcriptional pathway for cardiac hypertrophy. Cell. 1998;93:215–228.
14 Hofmann T, Schaefer M, Schultz G, Gudermann T. Transient receptor potential channels as molecular substrates of receptor-mediated cation entry. J Mol Med. 2000;78:14–25.
15 Montell C. The TRP superfamily of cation channels. Sci STKE. 2005;2005:re3.
16 Minke B, Cook B. TRP channel proteins and signal transduction. Physiol Rev. 2002;82:429–472.
17 Hofmann T, Obukhov AG, Schaefer M, Harteneck C, Gudermann T, Schultz G. Direct activation of human TRPC6 andTRPC3 channels by diacylglycerol. Nature. 1999;397:259–263.
18 Kuwahara K, Wang Y, McAnally J, Richardson JA, Bassel-Duby R, Hill JA, et al. TRPC6 fulfills a calcineurin signaling circuit

during pathologic cardiac remodeling. J Clin Invest. 2006;116: 3114–3126.
19 Kwan HY, Huang Y, Yao X. Regulation of canonical transient receptor potential isoform 3 (TRPC3) channel by protein kinase G. Proc Natl Acad Sci U S A. 2004;101:2625–2630.
20 Takahashi S, Lin H, Geshi N, Mori Y, Kawarabayashi Y, Takami N, et al. Nitric oxide-cgmp-protein kinase G pathway negatively regulates vascular transient receptor potential channel TRPC6. J Physiol. 2008;586:4209–4223.
21 Kinoshita H, Kuwahara K, Nishida M, Jian Z, Rong X, Kiyonaka S, et al. Inhibition of TRPC6 channel activity contributes to the antihypertrophic effects of natriuretic peptides-guanylyl cyclase-A signaling in the heart. Circ Res. 2010;106:1849–1860.
22 Tsutamoto T, Kanamori T, Morigami N, Sugimoto Y, Yamaoka O, Kinoshita M. Possibility of downregulation of atrial natriuretic peptide receptor coupled to guanylate cyclase in peripheral vascular beds of patients with chronic severe heart failure. Circulation. 1993;87:70–75.
23 Potter LR, Abbey-Hosch S, Dickey DM. Natriuretic peptides, their receptors, and cyclic guanosine monophosphate-dependent signaling functions. Endocr Rev. 2006;27:47–72.
24 Tarone G, Lembo G. Molecular interplay between mechanical and humoral signalling in cardiac hypertrophy. Trends Mol Med. 2003;9:376–382.
25 Brown JH, Del Re DP, Sussman MA. The Rac and Rho hall of fame: A decade of hypertrophic signaling hits. Circ Res. 2006; 98:730–742.
26 Lezoualc'h F, Metrich M, Hmitou I, Duquesnes N, Morel E. Small GTP-binding proteins and their regulators in cardiac hypertrophy. J Mol Cell Cardiol. 2008;44:623–632.
27 Parlakian A, Tuil D, Hamard G, Tavernier G, Hentzen D, Concordet JP, et al. Targeted inactivation of serum response factor in the developing heart results in myocardial defects and embryonic lethality. Mol Cell Biol. 2004;24:5281–5289.
28 Miano JM, Ramanan N, Georger MA, de Mesy Bentley KL, Emerson RL, Balza RO Jr, et al. Restricted inactivation of serum response factor to the cardiovascular system. Proc Natl Acad Sci U S A. 2004;101:17132–17137.
29 Zhang X, Azhar G, Chai J, Sheridan P, Nagano K, Brown T, et al. Cardiomyopathy in transgenic mice with cardiac-specific overexpression of serum response factor. Am J Physiol Heart Circ Physiol. 2001;280:H1782–H1792.
30 Nelson TJ, Balza R Jr, Xiao Q, Misra RP. SRF-dependent gene expression in isolated cardiomyocytes: Regulation of genes involved in cardiac hypertrophy. J Mol Cell Cardiol. 2005;39: 479–489.
31 Sprenkle AB, Murray SF, Glembotski CC. Involvement of multiple cis elements in basal- and alpha-adrenergic agonist-inducible atrial natriuretic factor transcription. Roles for serum response elements and an SP-1-like element. Circ Res. 1995;77:1060–1069.
32 Schneider MD, McLellan WR, Black FM, Parker TG. Growth factors, growth factor response elements, and the cardiac phenotype. Basic Res Cardiol. 1992;87 Suppl 2:33–48.
33 Gineitis D, Treisman R. Differential usage of signal transduction pathways defines two types of serum response factor target gene. J Biol Chem. 2001;276:24531–24539.
34 Hill CS, Wynne J, Treisman R. The rho family gtpases rhoa, rac1, and cdc42hs regulate transcriptional activation by srf. Cell. 1995;81:1159–1170.
35 Miralles F, Posern G, Zaromytidou AI, Treisman R. Actin dynamics control srf activity by regulation of its coactivator mal. Cell. 2003;113:329–342.
36 Kuwahara K, Barrientos T, Pipes GC, Li S, Olson EN. Muscle-specific signaling mechanism that links actin dynamics to serum response factor. Mol Cell Biol. 2005;25:3173–3181.
37 Kuwahara K, Kinoshita H, Kuwabara Y, Nakagawa Y, Usami S, Minami T, et al. Myocardin-related transcription factor A is a common mediator of mechanical stress- and neurohumoral stimulation-induced cardiac hypertrophic signaling leading to activation of brain natriuretic peptide gene expression. Mol Cell Biol. 2010;30:4134–4148.
38 Loirand G, Guerin P, Pacaud P. Rho kinases in cardiovascular physiology and pathophysiology. Circ Res. 2006;98:322–334.
39 Kuwahara K, Saito Y, Nakagawa O, Kishimoto I, Harada M, Ogawa E, et al. The effects of the selective ROCK inhibitor, Y27632, on ET-1-induced hypertrophic response in neonatal rat cardiac myocytes – possible involvement of Rho/ROCK pathway in cardiac muscle cell hypertrophy. FEBS Lett. 1999;452: 314–318.
40 Busche S, Descot A, Julien S, Genth H, Posern G. Epithelial cell-cell contacts regulate srf-mediated transcription via rac-actin-mal signalling. J Cell Sci. 2008;121:1025–1035.

Calcif Tissue Int (2012) 90:307–318
DOI 10.1007/s00223-011-9567-0

ORIGINAL RESEARCH

# Skeletal Analysis of the Long Bone Abnormality (*lbab/lbab*) Mouse, A Novel Chondrodysplastic C-Type Natriuretic Peptide Mutant

**Eri Kondo · Akihiro Yasoda · Takehito Tsuji · Toshihito Fujii · Masako Miura · Naotestu Kanamoto · Naohisa Tamura · Hiroshi Arai · Tetsuo Kunieda · Kazuwa Nakao**

Received: 5 July 2011 / Accepted: 22 December 2011 / Published online: 25 January 2012


**Abstract** Long bone abnormality (*lbab/lbab*) is a strain of dwarf mice. Recent studies revealed that the phenotype is caused by a spontaneous mutation in the *Nppc* gene, which encodes mouse C-type natriuretic peptide (CNP). In this study, we analyzed the chondrodysplastic skeletal phenotype of *lbab/lbab* mice. At birth, *lbab/lbab* mice are only slightly shorter than their wild-type littermates. Nevertheless, *lbab/lbab* mice do not undergo a growth spurt, and their final body and bone lengths are only ~60% of those of wild-type mice. Histological analysis revealed that the growth plate in *lbab/lbab* mice, especially the hypertrophic chondrocyte layer, was significantly thinner than in wild-type mice. Overexpression of CNP in the cartilage of *lbab/lbab* mice restored their thinned growth plate, followed by the complete rescue of their impaired endochondral bone growth. Furthermore, the bone volume in *lbab/lbab* mouse was severely decreased and was recovered by CNP overexpression. On the other hand, the thickness of the growth plate of *lbab/+* mice was not different from that of wild-type mice; accordingly, impaired endochondral bone growth was not observed in *lbab/+* mice. In organ culture experiments, tibial explants from fetal *lbab/lbab* mice were significantly shorter than those from *lbab/+* mice and elongated by addition of $10^{-7}$ M CNP to the same extent as *lbab/+* tibiae treated with the same dose of CNP. These results demonstrate that *lbab/lbab* is a novel mouse model of chondrodysplasia caused by insufficient CNP action on endochondral ossification.

**Keywords** C-type natriuretic peptide · Long bone abnormality (*lbab*) · Chondrodysplasia · Endochondral bone growth · Organ culture

C-type natriuretic peptide (CNP) is a member of the natriuretic peptide family and exerts its biological actions through the accumulation of intracellular cyclic GMP via a subtype of membranous guanylyl cyclase receptor, guanylyl cyclase-B (GC-B) [1, 2]. We previously demonstrated that the CNP/GC-B system is a potent stimulator of endochondral bone growth: transgenic mice with targeted overexpression of CNP in cartilage under the control of type II collagen promoter [3] or those with elevated plasma CNP concentrations under the control of human serum amyloid P component promoter [4] exhibit a prominent skeletal overgrowth phenotype. On the other hand, the physiological importance of the CNP/GC-B system on endochondral bone growth has been revealed by the phenotypes of hypomorphs. We generated complete CNP or GC-B null mice and demonstrated that they exhibit an impaired bone growth phenotype [5, 6]. We have also reported that in two lines of spontaneous mutant mice, *cn/cn* and *slw/slw*, disproportionate dwarfism is caused by loss-of-function mutations in the murine GC-B gene [7, 8].

The authors have stated that they have no conflict of interest.

**Electronic supplementary material** The online version of this article (doi:10.1007/s00223-011-9567-0) contains supplementary material, which is available to authorized users.

E. Kondo · A. Yasoda (✉) · T. Fujii · M. Miura · N. Kanamoto · N. Tamura · H. Arai · K. Nakao
Department of Medicine and Clinical Science, Kyoto University Graduate School of Medicine, Kyoto 606-8507, Japan
e-mail: yasoda@kuhp.kyoto-u.ac.jp

T. Tsuji · T. Kunieda
Department of Animal Science, Okayama University Graduate School of Natural Science and Technology, Okayama 700-8530, Japan

The skeletal phenotypes of these mutant mice resemble those of GC-B knockout mice. Furthermore, recent studies have elucidated that loss-of-function mutations in the human GC-B gene are the causes of acromesomelic dysplasia type Maroteaux (AMDM), one form of skeletal dysplasia with a disproportionate short stature phenotype [9]. The impaired skeletal growth phenotype observed in patients suffering from AMDM is similar to the skeletal phenotype of *cn/cn*, *slw/slw*, and GC-B knockout mice.

The long bone abnormality (*lbab/lbab*) mouse was first identified in The Jackson Laboratory (Bar Harbor, ME) as a spontaneous autosomal recessive mutant characterized by impaired growth of the long bones [10]. Recent studies have elucidated that the impaired growth of *lbab/lbab* mice is caused by a hypomorphic mutation in the CNP gene; Jiao et al. [11] found that its impaired growth phenotype is associated with a single point mutation in the mouse CNP gene, and we showed that this phenotype is completely recovered by CNP overexpression [12]. Yoder et al. [13] characterized the mutant CNP in *lbab/lbab* mice and demonstrated that it is less biologically active than authentic CNP; in whole-cell cGMP elevation and membrane guanylyl cyclase assays, 30-fold to greater than 100-fold more mutant CNP is required to activate GC-B compared to authentic CNP. We also confirmed that the mutant CNP in *lbab/lbab* mice retains only about 10% activity to induce cyclic GMP production through GC-B compared to authentic CNP in an in vitro transfection assay using COS-7 cells [12]. Collectively, *lbab/lbab* is a novel chondrodysplastic mouse model with insufficient CNP action on endochondral bone growth. Nevertheless, the skeletal phenotypes of *lbab/lbab* mice have only been partially described in short reports, including our own brief communication [11–13], and have not yet been fully studied. In this study, we performed further analyses of the skeletal phenotypes of *lbab/lbab* mice.

## Materials and Methods

### Mice

Heterozygous (*lbab/+*) mice (C57BL/6 J background) were obtained from The Jackson Laboratory, and the strain was maintained by sib mating of heterozygotes. Transgenic mice with targeted overexpression of CNP in the growth plate chondrocytes under the control of the mouse pro-$\alpha_1$(II) (*Col2a1*) promoter (CNP-Tg) were created as reported previously [3]. To perform genetic rescue of *lbab/lbab* mice, CNP-Tg mice were mated with *lbab/+* mice, and $F_1$ offspring heterozygous for the transgene and for the *lbab* allele were mated with those with only the *lbab* allele to generate *lbab/lbab* mice with the transgene expression (*lbab/lbab*·CNP-Tg/+ mice) [12]. Genotypes for the CNP transgene and the *lbab* allele were determined by PCR analysis using mouse genomic DNAs extracted from tails. Because there was no tendency of gender differences in the growth of each genotype (data not shown), we used only female mice in our experiments. Animal care and all experiments were conducted in accordance with the Guidelines for Animal Experiments of Kyoto University and were approved by the Animal Research Committee, Graduate School of Medicine, Kyoto University.

### Skeletal Analysis

For 10 weeks after birth, body lengths of female mice were measured weekly. Body length was measured as the length from the nose to the anus (nasoanal length) or that from the nose to the tip of the tail (nose–tail length). Body weights were also measured weekly. Skeletal analysis was performed as previously described [14]. Briefly, mice were subjected to soft X-ray analysis (30 kVp, 5 mA for 1 min; Softron type SRO-M5; Softron, Tokyo, Japan), and lengths of the bones were measured on the X-ray films. CT scanning of the humerus was performed using a ScanXmate-L090 Scanner (Comscantechno, Yokohama, Japan). Three-dimensional microstructural image data were reconstructed and structural indices calculated using TRI/3D-BON software (RATOC System Engineering, Tokyo, Japan).

### Histological Examination

Tibiae were fixed in 10% formalin neutral buffer, decalcified in 10% EDTA, and embedded in paraffin. Sections (5 μm thick) were sliced and stained with alcian blue (pH 2.5) and hematoxylin–eosin. For immunohistochemistry, sections were incubated with rabbit anti-type X collagen antibody (LSL, Tokyo, Japan), goat anti-Indian hedgehog (Ihh) antibody (Santa Cruz Biotechnology, Santa Cruz, CA), mouse anti-matrix metalloproteinase 13 (MMP-13) antibody (Thermo Fisher Scientific, Waltham, MA), and mouse anti–proliferating cell nuclear antigen (PCNA) antibody (Dako, Copenhagen, Denmark). Immunostaining was performed using the Histofine Mousestain Kit (Nichirei Biosciences, Tokyo, Japan) according to the manufacturer's instruction. Peroxidase activity was visualized using diaminobenzidine. Sections were counterstained with hematoxylin, dehydrated, and then mounted with malinol (Muto Pure Chemicals, Tokyo, Japan). To confirm antibody specificity, normal rabbit serum (Sigma-Aldrich, St. Louis, MO), normal goat IgG (Santa Cruz Biotechnology), and mouse IgG (Dako) were used as first antibodies for negative controls.

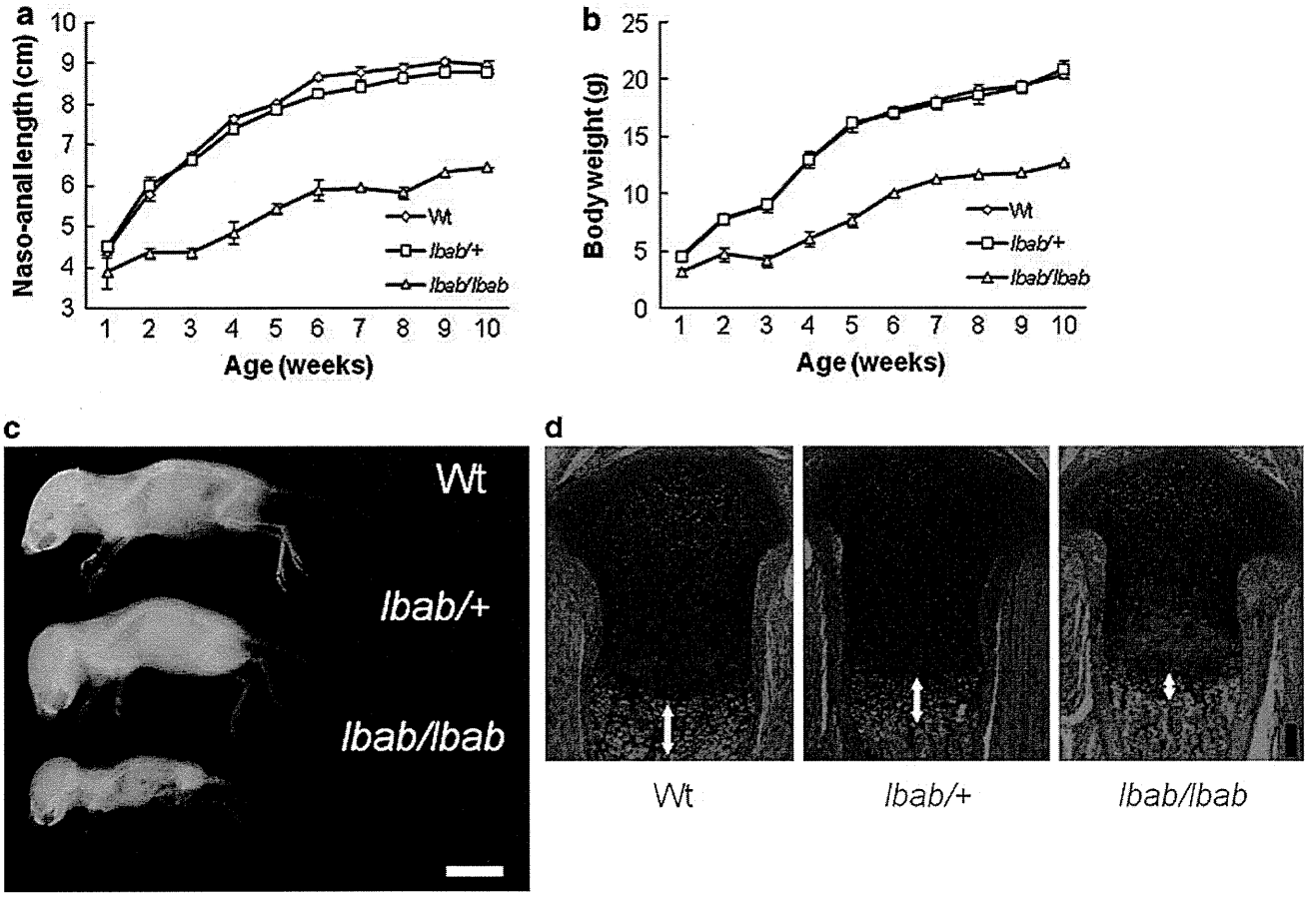


**Fig. 1** Growth and skeletal phenotype of *lbab/+* and *lbab/lbab* mice. Nasoanal lengths (**a**) and body weights (**b**) of female wild-type (*Wt, open diamond*), *lbab/+* (*open square*), and *lbab/lbab* (*open triangle*) mice ($n = 2$–8). **c** Whole skeletons of wild-type, *lbab/+* , and *lbab/lbab* mice at 2 weeks of age. *Scale bar* 1 cm. **d** Histological analysis of the tibial growth plates of 3-day-old mice. *Arrows* indicate hypertrophic chondrocyte layers. Alcian blue and hematoxylin–eosin staining. *Scale bar* 100 μm

### Organ Culture

Organ culture of fetal mouse tibiae or third metatarsi was performed as described previously [15]. Tibial or metatarsal explants from *lbab/+* mice and their *lbab/lbab* littermates at 16.5 days postcoitus were cultured for 4 days with vehicle or $10^{-7}$ M CNP (Peptide Institute, Minoh, Japan). Medium was changed every day. Before and after the culture, the maximal longitudinal lengths of tibiae were measured as the total tibial length, the sum of the lengths of proximal and distal cartilaginous primordia (CP), and the length of the osteogenic center (OC), using a linear ocular scale mounted on an inverted microscope. For histological analysis, explants were fixed in 10% formalin neutral buffer and embedded in paraffin. Sections (5 μm thick) were sliced and stained with alcian blue (pH 2.5) and hematoxylin–eosin. Immunohistochemical staining of incorporated bromodeoxyuridine (BrdU) was performed using 5-Bromo-2′-deoxyuridine labeling and detection kit II (Roche Applied Science, Indianapolis, IN) according to the manufacturer's protocol.

### Statistical Analysis

Data were expressed as the mean ± SEM. The statistical significance of differences between mean values was assessed using Student's *t*-test.

## Results

### Analyses of Skeletal Growth of *lbab/lbab* and *lbab/+* Mice

As previously reported, *lbab/lbab* mice developed severe dwarfism characterized by short tails and extremities [11, 12]. At birth, *lbab/lbab* pups were slightly shorter than their wild-type littermates: the nasoanal and nose–tail lengths of *lbab/lbab* mice were 88 and 83% of those of

their wild-type littermates, respectively (Fig. 1a, Supplemental Fig. 1).The ratios of nasoanal and nose–tail lengths of *lbab/lbab* mice to those of wild-type mice sharply decreased to 65% and 55%, respectively, by the age of 3 weeks. After 5 weeks of age, these ratios stabilized at 66–72% and 57–62%, respectively (Fig. 1a, Supplemental Fig. 1). The body weight of *lbab/lbab* mice was 68% of that of their wild-type littermates at birth and decreased to 46% by the age of 3 weeks. The ratio did not increase until 5 weeks of age, becoming ~60% after 7 weeks (Fig. 1b). On the other hand, *lbab/+* mice were indistinguishable from their wild-type littermates at birth and grew almost similarly (Fig. 1a,b, Supplemental Fig. 1). Soft X-ray analysis revealed that longitudinal growth of the vertebrae, tail, and extremities was affected in *lbab/lbab* mice at the age of 2 weeks but was not affected in *lbab/+* mice (Fig. 1c). Histological analysis revealed that at the age of 3 days the tibial growth plate, especially the hypertrophic chondrocyte layer, of *lbab/lbab* mice was apparently thinner than that of wild-type mice (Fig. 1d). On the other hand, the thickness of the tibial growth plate of *lbab/+* mice was not different from that of wild-type mice (Fig. 1d).

## Effect of CNP Overexpression on Impaired Endochondral Bone Growth of *lbab/lbab* Mice

In order to further characterize the impaired skeletal growth of *lbab/lbab* mice, we analyzed how their impaired endochondral bone growth recovered in response to targeted overexpression of CNP in the cartilage in vivo [12]. We crossed *lbab/lbab* mice with cartilage-specific CNP transgenic mice under the control of type II collagen promoter (CNP-Tg mice) and obtained *lbab/lbab* mice with transgenic expression of CNP in cartilage (*lbab/lbab*·CNP-Tg mice) [12]. At the first week after birth, the nasoanal length of *lbab/lbab*·CNP-Tg mice was almost the same as that of *lbab/lbab* mice and considerably smaller than that of wild-type mice: nasoanal lengths of wild-type, *lbab/lbab*, and *lbab/lbab*·CNP-Tg mice were 4.38 ± 0.06, 3.87 ± 0.37, and 4.00 ± 0.12 cm, respectively. Subsequently, *lbab/lbab*·CNP-Tg mice began to grow larger than *lbab/lbab* mice and promptly caught up with wild-type mice; although the nasoanal length of *lbab/lbab*·CNP-Tg mice was still considerably smaller than that of wild-type mice until 3 weeks of age (5.70 ± 0.57 and 6.71 ± 0.10 cm, respectively, at age 3 weeks), it became almost comparable to that of wild-type mice after 4 weeks (7.38 ± 0.48 and 7.61 ± 0.10 cm, respectively, at age 4 weeks). Further, the body weight of *lbab/lbab*·CNP-Tg mice was almost the same as that of *lbab/lbab* mice and smaller than that of wild-type mice until the age of 3 weeks but then promptly increased to a level comparable to that of wild-type mice (Supplemental Fig. 2).

Soft X-ray analyses revealed that at the age of 2 weeks the impaired growth of bones formed through endochondral ossification in *lbab/lbab* mice was partially recovered by targeted overexpression of CNP in cartilage in *lbab/lbab*·CNP-Tg mice (Fig. 2a): the recoveries in the longitudinal length of cranium and the lengths of the humerus, radius, ulna, femur, tibia, and vertebrae were 35, 73, 68, 37, 51, 63, and 27%, respectively (Fig. 2b). Furthermore, at the age of 10 weeks, the impaired endochondral bone growth in *lbab/lbab* mice was almost completely recovered by targeted overexpression of CNP in cartilage, as observed in *lbab/lbab*·CNP-Tg mice (Fig. 2c, d). On the other hand, there were no significant differences in the width of the cranium, which is formed via intramembranous ossification, among the three genotypes at either 2 or 10 weeks (Fig. 2b, d).

Histological analysis showed that the thickness of both the proliferative chondrocyte layer and the hypertrophic chondrocyte layer, positive for immunohistochemical staining for type X collagen, was significantly decreased in *lbab/lbab* mice compared to wild-type mice at the age of 2 weeks, as previously reported [12] (Fig. 3a, b).The thinner proliferative chondrocyte layer in the *lbab/lbab* growth plate was completely recovered by targeted overexpression of CNP as observed in the *lbab/lbab*·CNP-Tg growth plate (Fig. 3c). The thinner hypertrophic chondrocyte layer in the *lbab/lbab* growth plate was also considerably recovered in the *lbab/lbab*·CNP-Tg growth plate, although the extent of the recovery was less than in the proliferative chondrocyte layer (Fig. 3d). Immunohistochemical staining for PCNA revealed that the number of PCNA-positive cells was severely decreased in the proliferative chondrocyte layer of the *lbab/lbab* growth plate (Fig. 3e). The number of PCNA-positive cells did not recover in the proliferative chondrocyte layer of the *lbab/lbab*·CNP-Tg growth plate, whereas the thinner proliferative chondrocyte layer in the *lbab/lbab* growth plate was almost completely recovered in the *lbab/lbab*·CNP-Tg growth plate (Fig. 3c). The area positive for immunostaining of Ihh, one of the markers of hypertrophic differentiation, was decreased in the *lbab/lbab* growth plate compared to the wild-type growth plate (Fig. 3f). The smaller size of the area positive for Ihh in the *lbab/lbab* growth plate was almost completely recovered in the *lbab/lbab*·CNP-Tg growth plate (Fig. 3f). Immunohistochemical staining of MMP-13, a useful marker for terminal hypertrophic chondrocytes, was not changed between the three genotypes, indicating that the progression through the hypertrophy program was not accelerated in the *lbab/lbab* growth plate (Fig. 3g).

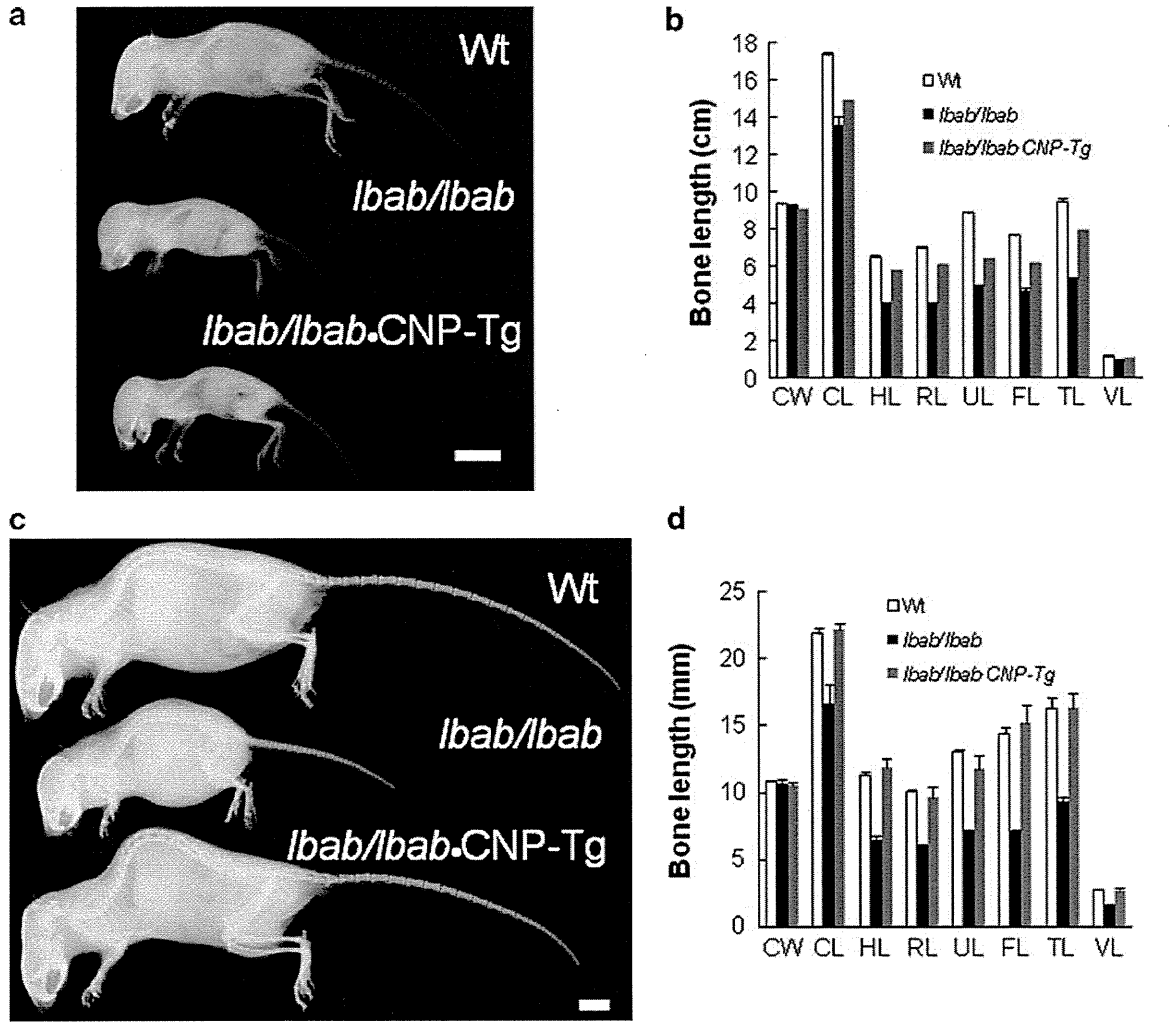


**Fig. 2** Effect of CNP overexpression on impaired endochondral bone growth of *lbab/lbab* mice. Whole skeletons (**a**, **c**) and bone lengths measured on soft X-ray films (**b**, **d**) of female wild-type (*Wt*), *lbab/lbab*, and *lbab/lbab*·CNP-Tg mice at the age of 2 weeks (**a**, **b**) and 10 weeks (**c**, **d**). **a**, **c** *Scale bar* 1 cm. **b**, **d** *White bars*, wild-type mice; *black bars*, *lbab/lbab* mice; *gray bars*, *lbab/lbab*·CNP-Tg mice. *CW*, width of cranium; *CL*, longitudinal length of cranium; *HL*, humeral length; *RL*, radial length; *UL*, ulnar length; *FL*, femoral length; *TL*, tibial length; *VL*, vertebral length. $n = 2$–7 (**b**) and 3–5 (**d**) (Color figure online)

At the age of 10 weeks, the tibial growth plate of *lbab/lbab* mice continued to be thinner than that of wild-type mice and was completely recovered by overexpression of CNP in cartilage (Fig. 4).

## Recovery of Decreased Bone Volume in *lbab/lbab* Mouse by CNP Overexpression

Three-dimensional CT analysis manifested a marked reduction in bone volume of the humerus in *lbab/lbab* mice and considerable recovery in *lbab/lbab*·CNP-Tg mice (Fig. 5). At the age of 10 weeks, the quantified bone volume (BV/TV) and trabecular thickness (Tb.Th) of the humerus in *lbab/lbab* mice were 2.4% and 34.5 μm, whereas those in wild-type mice were 4.1% and 40.3 μm, respectively. The decreased BV/TV and Tb.Th in *lbab/lbab* mice were increased to 5.4% and 37.0 μm, respectively, in *lbab/lbab*·CNP-Tg mice.

## Organ Culture Experiments of Tibiae from *lbab/lbab* Mice

In order to further analyze the impaired endochondral ossification of *lbab/lbab* mice, we preformed organ culture experiments using tibial explants from fetal mice (Fig. 6a) [15]. Because skeletal phenotypes of mice heterozygous for the *lbab* allele were not different from those of wild-type mice, we compared the growth of tibial explants from *lbab/lbab* mice with that from *lbab/+* mice. At the beginning of culture, both the total length and the sum length of the CP of *lbab/lbab* tibiae were significantly smaller than those of *lbab/+* tibiae (3.80 ± 0.04

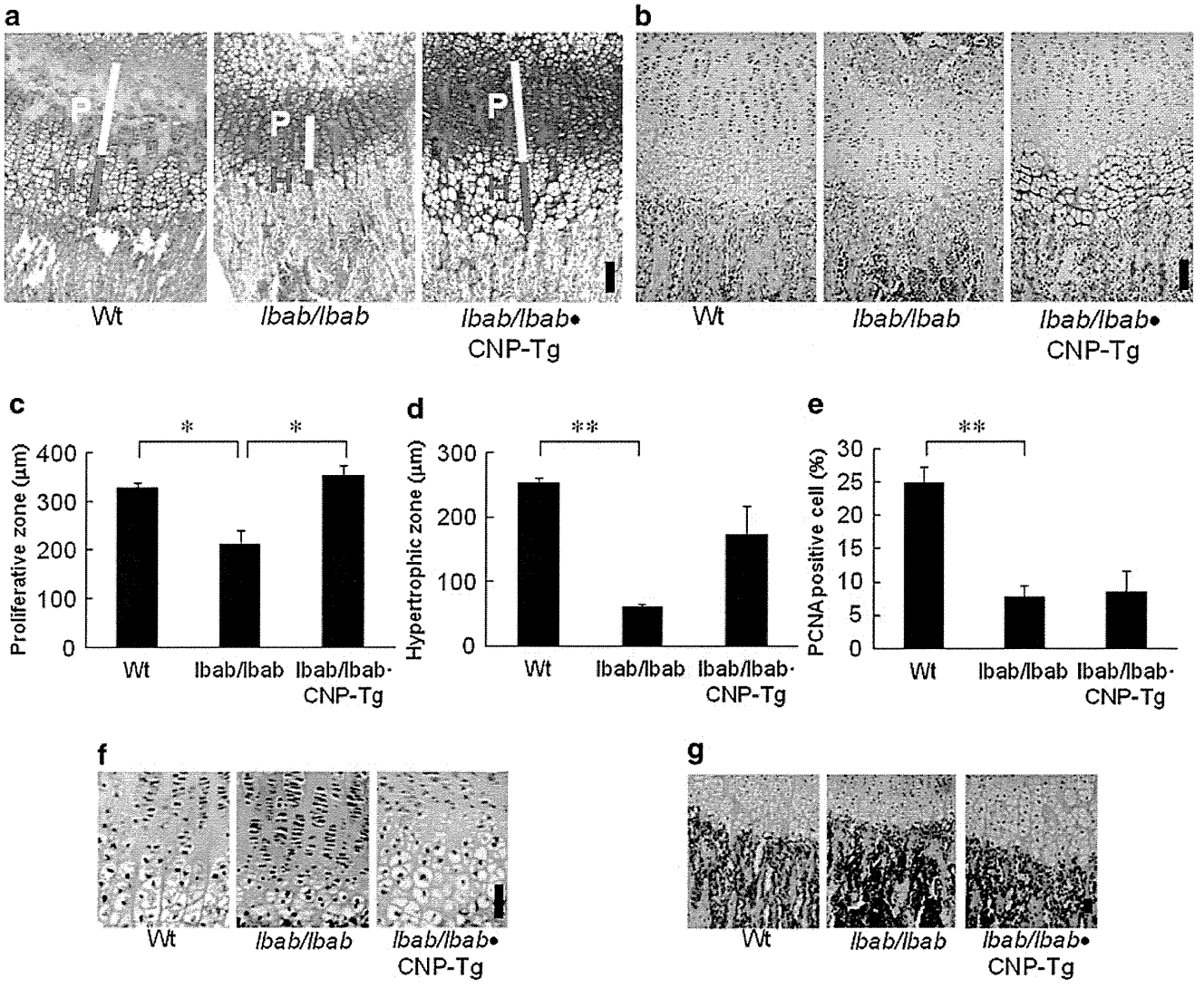


**Fig. 3** Histological analysis of tibial growth plates from 2-week-old wild-type (*Wt*), *lbab/lbab*, and *lbab/lbab*·CNP-Tg mice. **a** Alcian blue and hematoxylin–eosin staining. *Yellow bars* (depicted as *P*) indicate proliferative chondrocyte layers, and *red bars* (depicted as *H*) indicate hypertrophic chondrocyte layers. **b** Immunohistochemical staining for type X collagen. Scale bar in **a** and **b** = 100 μm. Heights of the proliferative (**c**) and hypertrophic (**d**) chondrocyte layers. $n = 3$ each. $^{*}P < 0.05$, $^{**}P < 0.01$. **e** The proportion of PCNA-positive chondrocytes in proliferative chondrocyte layers. $n = 3$–4. $^{**}P < 0.01$. Immunohistochemical staining of Ihh (**f**) and MMP-13 (**g**). Scale bar in **f** and **g** = 50 μm

vs. 4.25 ± 0.03 and 2.19 ± 0.02 vs. 2.43 ± 0.01 mm, respectively, $n = 8$–12 each) (Fig. 6b, c). Tibial explants from *lbab/lbab* mice grew to the same extent as those from *lbab/+* mice during a 4-day culture period; the difference in the total length or in the length of the CP between *lbab/lbab* and *lbab/+* explants at the end of culture was comparable to that at the beginning of culture (Fig. 6b, c). There was no significant difference in the length of the OC between the two genotypes before and after the culture period (data not shown).

The treatment of CNP at the dose of $10^{-7}$ M stimulated the growth of both *lbab/lbab* and *lbab/+* tibiae (Fig. 6b, c). CNP stimulated the growth of *lbab/lbab* tibiae more potently than that of *lbab/+* tibiae; in the presence of $10^{-7}$ M CNP, the difference between the total length of *lbab/+* tibiae and that of *lbab/lbab* tibiae was decreased (Fig. 6b), and furthermore, the CP length of *lbab/lbab* tibiae became almost the same as that of *lbab/+* tibiae (Fig. 6c). The growth of the OC was not stimulated by CNP in either *lbab/lbab* or *lbab/+* explants (data not shown).

Histological examination at the end of the culture period revealed that the length of the primordial growth plate (Fig. 7a), especially that of the hypertrophic chondrocyte layer positive for type X collagen immunostaining (Fig. 7b,c), was smaller in *lbab/lbab* explants than in

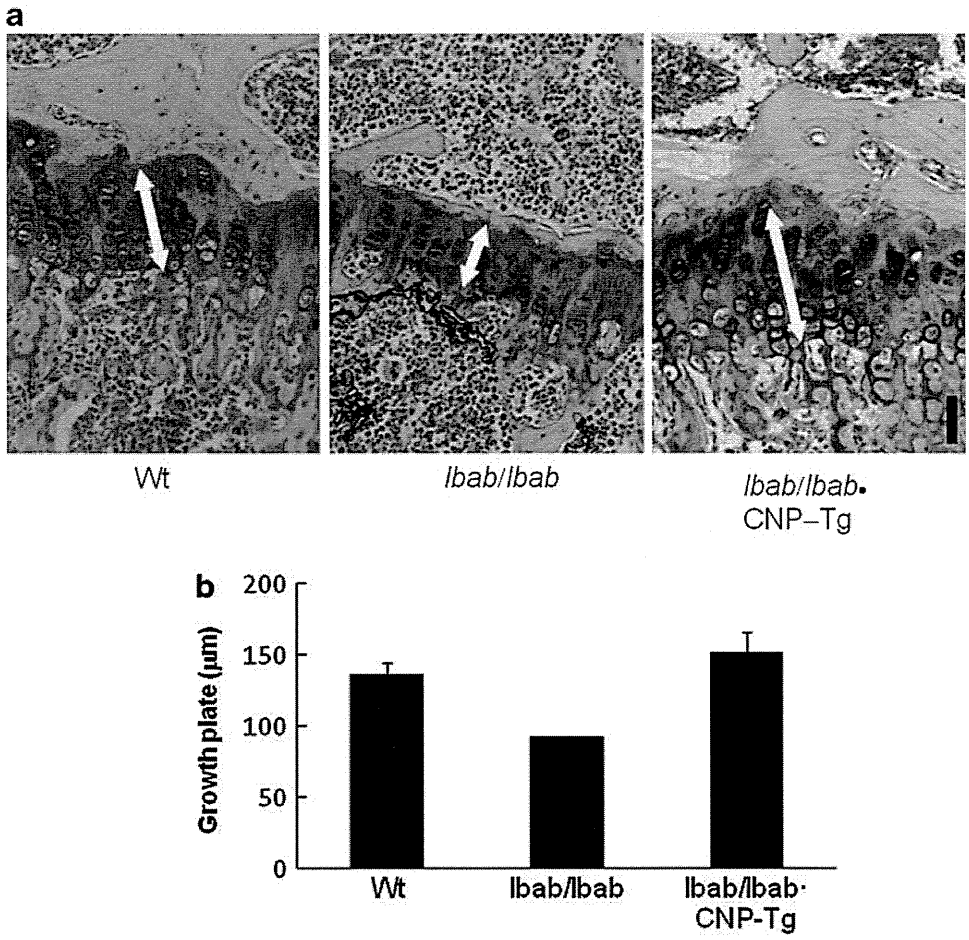


**Fig. 4** Histological analysis of tibial growth plate from female 10-week-old wild-type (*Wt*), *lbab/lbab*, and *lbab/lbab*·CNP-Tg mice. **a** Alcian blue and hematoxylin–eosin staining. *Arrows* indicate the width of growth plates. *Scale bar* 50 μm. **b** Total heights of the growth plates. $n = 2$–5 each

*lbab/+* explants. The area positive for immunostaining for Ihh, one of the markers for chondrogenic differentiation [16], tended to be a little decreased in *lbab/lbab* explants compared to that in *lbab/+* explants, although the intensity of the immunostaining was not different between the two genotypes (Supplemental Fig. 3). Immunohistochemical detection of BrdU-incorporated chondrocytes revealed that BrdU-positive chondrocytes tended to be decreased in *lbab/lbab* explants compared to those in *lbab/+* explants (Fig. 7d). Addition of CNP prominently increased the lengths of primordial growth plates (Fig. 7a) and their hypertrophic chondrocyte layers (Fig. 7b, c) of both *lbab/+* and *lbab/lbab* explants. The lengths of the primordial growth plate and its hypertrophic chondrocyte layer of *lbab/lbab* explants treated with $10^{-7}$ M CNP became comparable to those of *lbab/+* explants treated with the same dose of CNP (Fig. 7a–c). CNP increased the areas positive for Ihh immunostaining in both *lbab/+* and *lbab/lbab* explants. By addition of CNP, the sizes of the areas positive for, and the intensities of, Ihh immunostaining were not different between *lbab/+* and *lbab/lbab* explants (Supplemental Fig. 3). CNP did not increase BrdU-positive chondrocytes in *lbab/lbab* explants (Fig. 7d).

Further, we explored whether CNP controls the progression of growth plate chondrocytes through the different stages of maturation or not. Because the process of endochondral ossification is delayed in the metatarsus compared to that in the tibia in an individual, we performed organ culture of metatarsi as well as tibiae from fetal mice at 16.5-days postcoitus and examined the expression of type X collagen and Ihh. In the case of *lbab/+* organ culture, the area positive for immunostaining of type X collagen was reduced and that of Ihh was localized near the ossification center in metatarsal explants compared with those in tibial explants, indicating that the metatarsal growth plate represents an earlier stage of endochondral ossification than the tibial growth plate (Fig. 8). The area positive for immunostaining of type X collagen was greatly reduced in *lbab/lbab* metatarsal explants compared with that in *lbab/+* metatarsal explants and recovered by addition of $10^{-7}$ M CNP to the same extent to that in *lbab/+* metatarsal explants treated with vehicle. The area positive for immunostaining of Ihh became closer to ossification center


**Fig. 5** Micro-CT analysis of humeri from wild-type (*Wt*), *lbab/lbab*, and *lbab/lbab*·CNP-Tg mice at the age of 10 weeks. *Scale bar* 1 mm

in *lbab/lbab* metatarsal explants than in *lbab*/+ metatarsal explants and was returned to the same position as *lbab*/+ metatarsal explants by addition of CNP (Fig. 8).

## Discussion

Previously, we and other groups had reported in brief communications that the short stature phenotype of *lbab/lbab* mice is caused by a mutation in the CNP gene [11–13]. Here, we further analyzed the skeletal phenotypes of *lbab/lbab* mice and report the results in this full-length article.

Analysis of the growth curves of nasoanal and nose–tail lengths revealed that the shortness of *lbab/lbab* mice is mild at birth but rapidly progresses by the age of 3 weeks, and then, after 4 weeks, the ratio of the length of *lbab/lbab* mice compared to that of wild-type mice becomes almost constant. This suggests that CNP is especially crucial for the skeletal growth spurt that occurs in early life. Since CNP is expressed in the growth plate cartilage and works as an autocrine/paracrine regulator [5], CNP might affect the endochondral bone growth potently when the volume of growth plate cartilage is relatively abundant.

We confirmed the thinness of the growth plate of *lbab/lbab* mice, especially in its hypertrophic chondrocyte layer, followed by the impaired growth of long bones. The thinness of the growth plate of *lbab/lbab* mice was almost completely recovered by targeted overexpression of CNP in the growth plate by the age of 2 weeks. On the other hand, the recovery of the shortness of the total length of *lbab/lbab* bones by CNP was only partial at 2 weeks, becoming complete at the age of 10 weeks. This finding suggests that the recovery is evident earlier in the thickness of the growth plate than in the total bone length. In addition, immunohistochemistry for PCNA revealed that at the age of 2 weeks the proliferation of growth plate chondrocytes is decreased in *lbab/lbab* mice and that the decreased proliferation is not rescued by CNP overexpression, even though the thickness of the growth plate does fully recover.

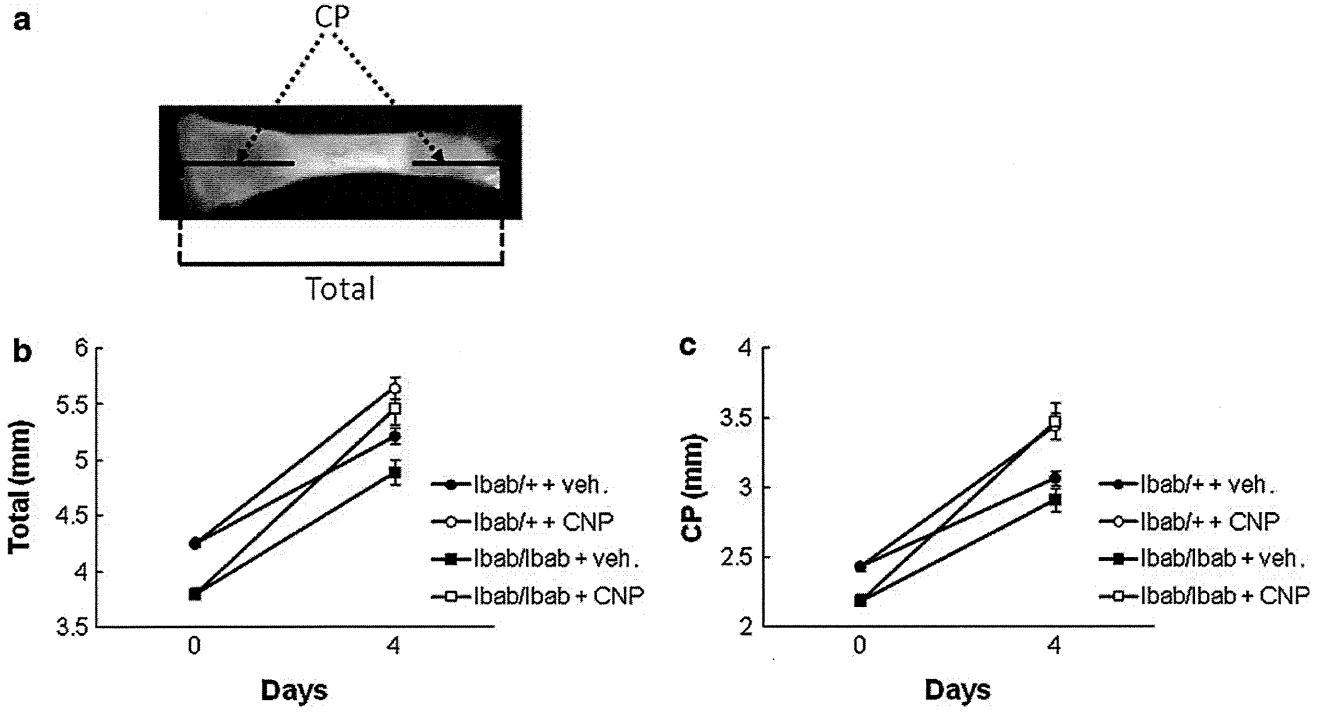


**Fig. 6** Effect of CNP on cultured tibiae from fetal *lbab/+* and *lbab/lbab* mice. **a** A representative picture of a tibial explant from a fetal mouse. Total longitudinal length (*Total*) and the sum lengths of cartilaginous primordia (*CP*) are indicated. Graphs of total (**b**) and CP (**c**) lengths of cultured tibiae from *lbab/+* and *lbab/lbab* mice treated with vehicle (*veh.*) or $10^{-7}$ M CNP (*CNP*) for 4 days. *Circles* indicate *lbab/+* tibiae, and *squares* indicate *lbab/lbab* tibiae. At the end of culture, *closed symbols* indicate tibiae treated with vehicle and *open symbols* indicate those treated with CNP. $n = 8$–12 each

The reason the decreased proliferation of chondrocytes in the *lbab/lbab* growth plate was not rescued by CNP overexpression in chondrocytes is not clear, but it may be because of the weak and slow expression of the CNP transgene owing to the weak power of the promoter region. On the other hand, CNP could not increase the proliferation of growth plate chondrocytes in *lbab/lbab* explants in organ culture experiments in this study. The effect of CNP on chondrocyte proliferation might be so mild that other effects of CNP on growth plate chondrocytes, e.g., the stimulatory effect on matrix synthesis as we had previously reported [3, 4], might proceed to recover the thinned growth plate of *lbab/lbab* mice. The discrepancy between the effects on proliferation and matrix synthesis may explain in part the delayed recovery of bone length relative to growth plate thickness. On the other hand, immunohistochemical staining of type X collagen and Ihh in explanted growth plates at two different stages of endochondral ossification suggested that the progression of proliferative chondrocytes to hypertrophic chondrocytes was delayed in the *lbab/lbab* growth plate and recovered by addition of CNP. In addition to the result that the expression of MMP-13 was not different between the terminal hypertrophic chondrocytes of wild-type, *lbab/lbab*, and rescued growth plates, CNP might promote the hypertrophic differentiation of proliferative chondrocytes but not accelerate the terminal differentiation of hypertrophic chondrocytes.

In this study, we investigated the character of calcified bones of *lbab/lbab* mice using three-dimensional CT analysis: the bone volume of *lbab/lbab* mice was substantially decreased compared to that of wild-type mice and recovered by cartilage-specific CNP overexpression. The mechanism of decrease in bone volume of *lbab/lbab* mice is still unknown, but CNP may be expressed in and affect cells other than chondrocytes, i.e., osteoblasts or osteoclasts, in bone. Although overexpression of CNP was targeted to chondrocytes in our rescue experiments, early onset of CNP-Tg expression from the CP might have been able to affect bone metabolism at the earlier stage of skeletogenesis [17] and may have continued to affect osteoblasts or osteoclasts near the growth plate cartilage in the later stage of skeletogenesis. Whereas several in vitro effects of CNP on osteoblastic cell lineages or osteoclasts have been reported [18–28], the in vivo effects of CNP on bone metabolism remain elusive; and further experiments are now ongoing in our laboratory.

We previously discovered that in two strains of mice, *cn/cn* and *slw/slw*, dwarfism is caused by spontaneous

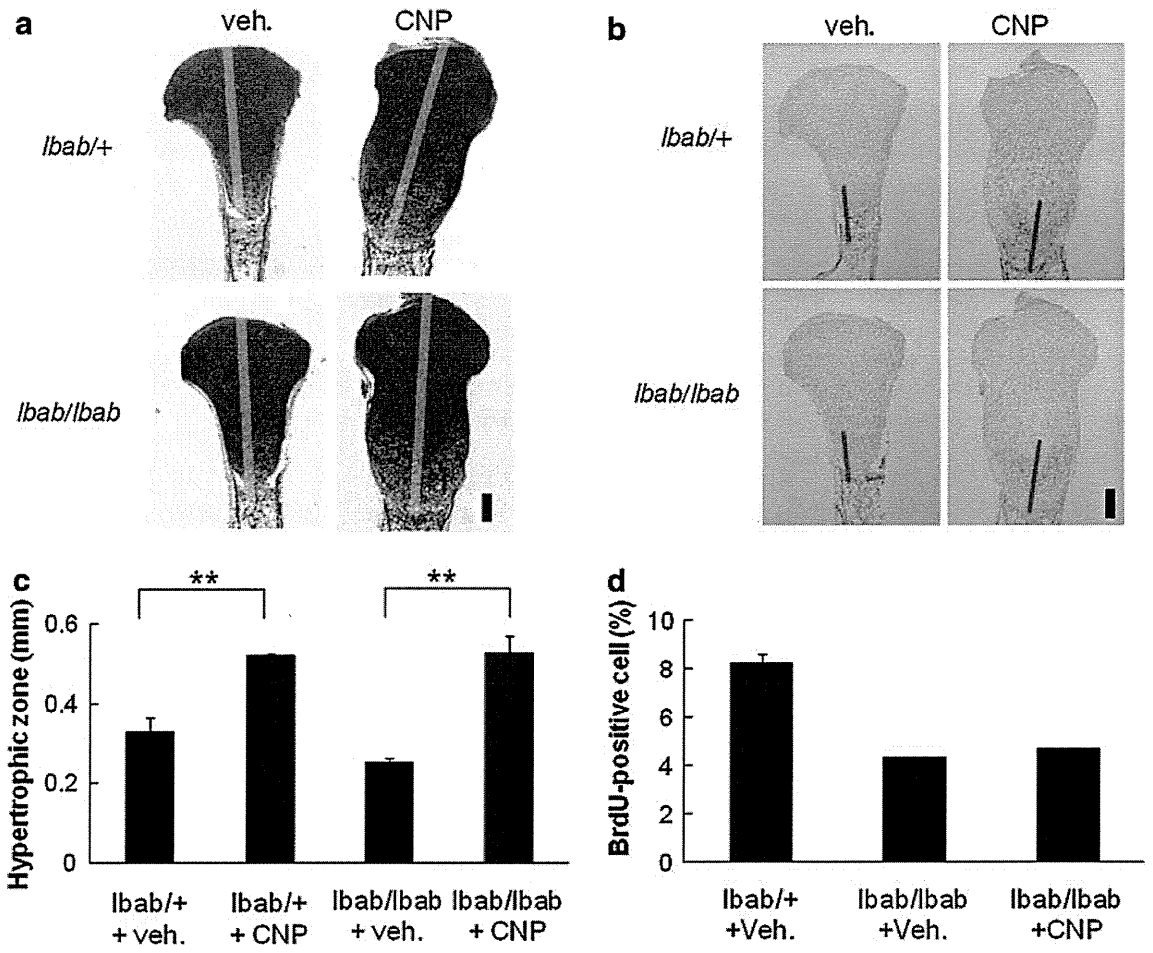


**Fig. 7** Histological analyses of the growth plates of tibial explants from fetal *lbab/+* and *lbab/lbab* mice treated with vehicle (*veh.*) or $10^{-7}$ M CNP (*CNP*) for 4 days. Alcian blue and hematoxylin–eosin staining (**a**) and immunohistochemical staining for type X collagen (**b**). *Yellow bars* in **a** indicate lengths of cartilaginous primordial, and *red bars* in **b** indicate heights of hypertrophic chondrocyte layers. *Scale bars* 200 μm. Height of hypertrophic chondrocyte layer (**c**) and proportion of BrdU-positive cells (**d**) of the growth plate of tibial explant from fetal *lbab/+* or *lbab/lbab* mice treated with $10^{-7}$ M CNP or vehicle at the end of the 4-day culture period. $n = 3$ each. $^{**}P < 0.01$ in **c** and $n = 2$–3 each in **d** (Color figure online)

mutations in the GC-B gene [7, 8]. In humans, it has been identified that AMDM is caused by spontaneous loss-of-function mutations in the GC-B gene [9, 29]. The *lbab/lbab* mouse, the skeletal phenotype of which we have closely analyzed in the present report, has a spontaneous loss-of-function mutation in the CNP gene; by analogy to the GC-B gene, some forms of human skeletal dysplasia might be caused by mutations in the CNP gene. Thus far, no such conditions have been discovered [30]. In the event such a discovery is made, the *lbab/lbab* mouse would then be a novel model of a form of human skeletal dysplasia caused by a mutation in the CNP gene.

In contrast to mice homozygous for the *lbab* allele, the growth and skeletal phenotype of mice heterozygous for the *lbab* allele were not different from those of wild-type mice, as is the case with heterozygous CNP knockout mice. This confirms that haploinsufficiency for the CNP gene does not exist in mice. Likewise, heterozygotes for the GC-B knockout, the *cn* allele, or the *slw* allele exhibit no skeletal abnormalities [6–8]; thus, haploinsufficiency of the GC-B gene also does not exist in mice. Nevertheless, haploinsufficiency of the GC-B gene does exist in humans: heterozygous carriers of AMDM are reported to be shorter than expected for their population of origin [31]. The reason for the discrepancy is not clear at present, but it may have to do with differences between species or some other unknown mechanism(s). We will have to perform further investigations on the skeletal phenotypes of the aforementioned lines of GC-B mutant mice; such experiments are now ongoing in our laboratory.

In summary, in this study we more closely investigated the skeletal phenotypes of a novel CNP mutant mouse, *lbab/lbab*. The results of this study will be useful not only for further elucidation of the physiological role of CNP on

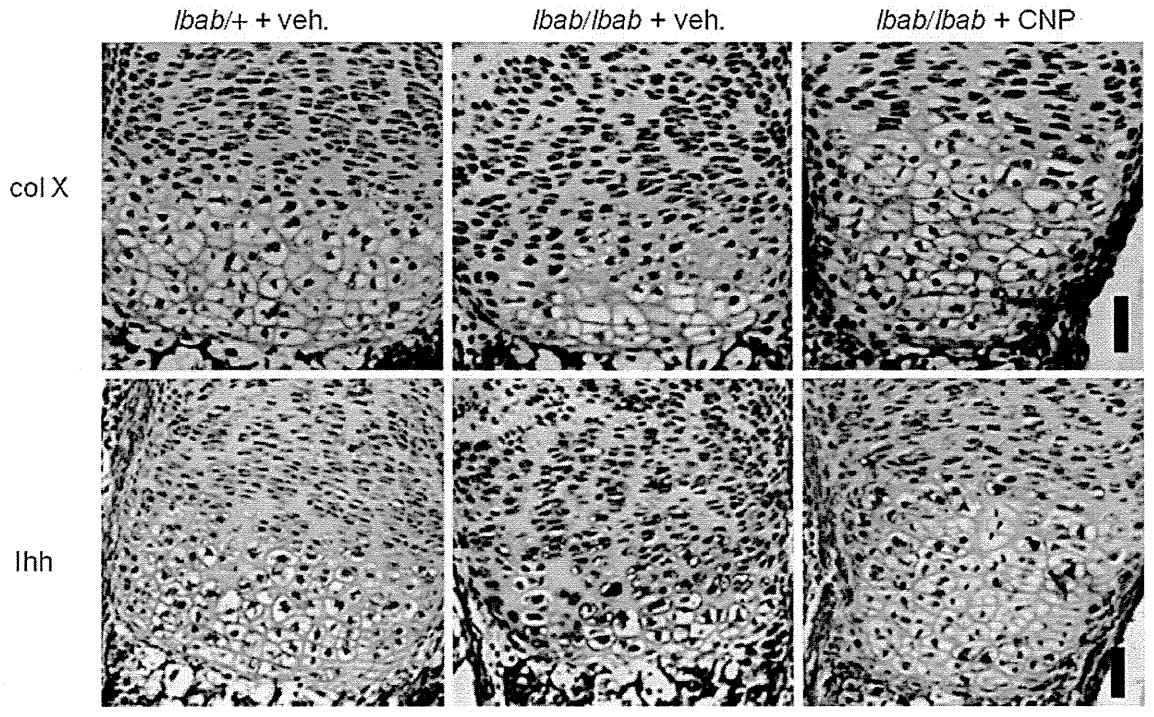


**Fig. 8** Immunohistochemical staining of type X collagen (*upper panels*) and Ihh (*lower panels*) of the growth plates of metatarsal explants from fetal *lbab/+* and *lbab/lbab* mice treated with vehicle (*veh.*) or $10^{-7}$ M CNP for 4 days. *Scale bar* 50 μm

endochondral bone growth but also for the prediction of pathophysiology of a hypothetical chondrodysplasia caused by a mutation in the human CNP gene, which has not yet been discovered.

**Acknowledgments** We thank B. de Crombrugghe (Department of Genetics, University of Texas M.D. Anderson Cancer Center) for the *Col2a1* promoter. This study was supported by a Grant-in-Aid for Scientific Research from the Ministry of Health, Labor, and Welfare of Japan and the Ministry of Education, Culture, Sports, Sciences, and Technology of Japan (21591176, 21119013).

## References

1. Nakao K, Ogawa Y, Suga S, Imura H (1992) Molecular biology and biochemistry of the natriuretic peptide system. I: Natriuretic peptides. J Hypertens 10:907–912
2. Nakao K, Ogawa Y, Suga S, Imura H (1992) Molecular biology and biochemistry of the natriuretic peptide system. II: Natriuretic peptide receptors. J Hypertens 10:1111–1114
3. Yasoda A, Komatsu Y, Chusho H, Miyazawa T, Ozasa A, Miura M, Kurihara T, Rogi T, Tanaka S, Suda M, Tamura N, Ogawa Y, Nakao K (2004) Overexpression of CNP in chondrocytes rescues achondroplasia through a MAPK-dependent pathway. Nat Med 10:80–86
4. Kake T, Kitamura H, Adachi Y, Yoshioka T, Watanabe T, Matsushita H, Fujii T, Kondo E, Tachibe T, Kawase Y, Jishage K, Yasoda A, Mukoyama M, Nakao K (2009) Chronically elevated plasma C-type natriuretic peptide level stimulates skeletal growth in transgenic mice. Am J Physiol Endocrinol Metab 297:E1339–E1348
5. Chusho H, Tamura N, Ogawa Y, Yasoda A, Suda M, Miyazawa T, Nakamura K, Nakao K, Kurihara T, Komatsu Y, Itoh H, Tanaka K, Saito Y, Katsuki M, Nakao K (2001) Dwarfism and early death in mice lacking C-type natriuretic peptide. Proc Natl Acad Sci USA 98:4016–4021
6. Tamura N, Doolittle LK, Hammer RE, Shelton JM, Richardson JA, Garbers DL (2004) Critical roles of the guanylyl cyclase B receptor in endochondral ossification and development of female reproductive organs. Proc Natl Acad Sci USA 101:17300–17305
7. Tsuji T, Kunieda T (2005) A loss-of-function mutation in natriuretic peptide receptor 2 (*Npr2*) gene is responsible for disproportionate dwarfism in *cn/cn* mouse. J Biol Chem 280: 14288–14292
8. Sogawa C, Tsuji T, Shinkai Y, Katayama K, Kunieda T (2007) Short-limbed dwarfism: *slw* is a new allele of Npr2 causing chondrodysplasia. J Hered 98:575–580
9. Bartels CF, Bükülmez H, Padayatti P, Rhee DK, van Ravenswaaij-Arts C, Pauli RM, Mundlos S, Chitayat D, Shih LY, Al-Gazali LI, Kant S, Cole T, Morton J, Cormier-Daire V, Faivre L, Lees M, Kirk J, Mortier GR, Leroy J, Zabel B, Kim CA, Crow Y, Braverman NE, van den Akker F, Warman ML (2004) Mutations in the transmembrane natriuretic peptide receptor NPR-B impair skeletal growth and cause acromesomelic dysplasia, type Maroteaux. Am J Hum Genet 75:27–34
10. The Jackson Laboratory. http://www.jax.org/index.html
11. Jiao Y, Yan J, Jiao F, Yang H, Donahue LR, Li X, Roe BA, Stuart J, Gu W (2007) A single nucleotide mutation in Nppc is associated with a long bone abnormality in *lbab* mice. BMC Genet 8:16
12. Tsuji T, Kondo E, Yasoda A, Inamoto M, Kiyosu C, Nakao K, Kunieda T (2008) Hypomorphic mutation in mouse *Nppc* gene

causes retarded bone growth due to impaired endochondral ossification. Biochem Biophys Res Commun 376:186–190
13. Yoder AR, Kruse AC, Earhart CA, Ohlendorf DH, Potter LR (2008) Reduced ability of C-type natriuretic peptide (CNP) to activate natriuretic peptide receptor B (NPR-B) causes dwarfism in *lbab-/-* mice. Peptides 29:1575–1581
14. Suda M, Ogawa Y, Tanaka K, Tamura N, Yasoda A, Takigawa T, Uehira M, Nishimoto H, Itoh H, Saito Y, Shiota K, Nakao K (1998) Skeletal overgrowth in transgenic mice that overexpress brain natriuretic peptide. Proc Natl Acad Sci USA 95:2337–2342
15. Yasoda A, Ogawa Y, Suda M, Tamura N, Mori K, Sakuma Y, Chusho H, Shiota K, Tanaka K, Nakao K (1998) Natriuretic peptide regulation of endochondral ossification. Evidence for possible roles of the C-type natriuretic peptide/guanylyl cyclase-B pathway. J Biol Chem 273:11695–11700
16. Vortkamp A, Lee K, Lanske B, Segre GV, Kronenberg HM, Tabin CJ (1996) Regulation of rate of cartilage differentiation by Indian hedgehog and PTH-related protein. Science 273:613–622
17. Zhou G, Garofalo S, Mukhopadhyay K, Lefebvre V, Smith CN, Eberspaecher H, de Crombrugghe B (1995) A 182 bp fragment of the mouse pro alpha 1(II) collagen gene is sufficient to direct chondrocyte expression in transgenic mice. J Cell Sci 108(Pt 12): 3677–3684
18. Inoue A, Hiruma Y, Hirose S, Yamaguchi A, Furuya M, Tanaka S, Hagiwara H (1996) Stimulation by C-type natriuretic peptide of the differentiation of clonal osteoblastic MC3T3-E1 cells. Biochem Biophys Res Commun 221:703–707
19. Hagiwara H, Inoue A, Yamaguchi A, Yokose S, Furuya M, Tanaka S, Hirose S (1996) cGMP produced in response to ANP and CNP regulates proliferation and differentiation of osteoblastic cells. Am J Physiol Cell Physiol 270:C1311–C1318
20. Suda M, Tanaka K, Fukushima M, Natsui K, Yasoda A, Komatsu Y, Ogawa Y, Itoh H, Nakao K (1996) C-type natriuretic peptide as an autocrine/paracrine regulator of osteoblast. Evidence for possible presence of bone natriuretic peptide system. Biochem Biophys Res Commun 223:1–6
21. Yanaka N, Akatsuka H, Kawai E, Omori K (1998) 1,25-Dihydroxyvitamin $D_3$ upregulates natriuretic peptide receptor-C expression in mouse osteoblasts. Am J Physiol Endocrinol Metab 275:E965–E973
22. Inoue A, Hayakawa T, Otsuka E, Kamiya A, Suzuki Y, Hirose S, Hagiwara H (1999) Correlation between induction of expression of biglycan and mineralization by C-type natriuretic peptide in osteoblastic cells. J Biochem 125:103–108
23. Suda M, Komatsu Y, Tanaka K, Yasoda A, Sakuma Y, Tamura N, Ogawa Y, Nakao K (1999) C-type natriuretic peptide/guanylate cyclase B system in rat osteogenic ROB-C26 cells and its down-regulation by dexamethazone. Calcif Tissue Int 65:472–478
24. Inoue A, Kamiya A, Ishiji A, Hiruma Y, Hirose S, Hagiwara H (2000) Vasoactive peptide-regulated gene expression during osteoblastic differentiation. J Cardiovasc Pharmacol 36:S286–S289
25. Inoue A, Kobayashi Y, Ishizuka M, Hirose S, Hagiwara H (2002) Identification of a novel osteoblastic gene, inducible by C-type natriuretic peptide, whose transcript might function in mineralization as a noncoding RNA. Calcif Tissue Int 70:111–116
26. Yeh LC, Zavala MC, Lee JC (2006) C-type natriuretic peptide enhances osteogenic protein-1-induced osteoblastic cell differentiation via Smad5 phosphorylation. J Cell Biochem 97:494–500
27. Kaneki H, Kurokawa M, Ide H (2008) The receptor attributable to C-type natriuretic peptide-induced differentiation of osteoblasts is switched from type B- to type C-natriuretic peptide receptor with aging. J Cell Biochem 103:753–764
28. Holliday LS, Dean AD, Greenwald JE, Glucks SL (1995) C-type natriuretic peptide increases bone resorption in 1,25-dihydroxyvitamin $D_3$–stimulated mouse bone marrow cultures. J Biol Chem 270:18983–18989
29. Hachiya R, Ohashi Y, Kamei Y, Suganami T, Mochizuki H, Mitsui N, Saitoh M, Sakuragi M, Nishimura G, Ohashi H, Hasegawa T, Ogawa Y (2007) Intact kinase homology domain of natriuretic peptide receptor-B is essential for skeletal development. J Clin Endocrinol Metab 92:4009–4014
30. Superti-Furga A, Unger S (2007) Nosology and classification of genetic skeletal disorders: 2006 revision. Am J Med Genet A 143:1–18
31. Olney RC, Bükülmez H, Bartels CF, Prickett TC, Espiner EA, Potter LR, Warman ML (2006) Heterozygous mutations in natriuretic peptide receptor-B (NPR2) are associated with short stature. J Clin Endocrinol Metab 91:1229–1232

# Forkhead Box A1 (FOXA1) and A2 (FOXA2) Oppositely Regulate Human Type 1 Iodothyronine Deiodinase Gene in Liver

Naotetsu Kanamoto, Tetsuya Tagami, Yoriko Ueda-Sakane, Masakatsu Sone, Masako Miura, Akihiro Yasoda, Naohisa Tamura, Hiroshi Arai, and Kazuwa Nakao

Department of Medicine and Clinical Science, Kyoto University Graduate School of Medicine (N.K., Y.U.-S., M.S., M.M., A.Y., N.T., H.A., K.N.), Kyoto 606-8507, Japan; and Division of Endocrinology and Metabolism, Clinical Research Institute, National Hospital Organization Kyoto Medical Center (T.T.), Kyoto 612-8555, Japan

Type 1 iodothyronine deiodinase (D1), a selenoenzyme that catalyzes the bioactivation of thyroid hormone, is expressed mainly in the liver. Its expression and activity are modulated by several factors, but the precise mechanism of its transcriptional regulation remains unclear. In the present study, we have analyzed the promoter of human D1 gene (*hDIO1*) to identify factors that prevalently increase D1 activity in the human liver. Deletion and mutation analyses demonstrated that a forkhead box (FOX)A binding site and an E-box site within the region between nucleotides −187 and −132 are important for *hDIO1* promoter activity in the liver. EMSA demonstrated that FOXA1 and FOXA2 specifically bind to the FOXA binding site and that upstream stimulatory factor (USF) specifically binds to the E-box element. Overexpression of FOXA2 decreased *hDIO1* promoter activity, and short interfering RNA-mediated knockdown of FOXA2 increased the expression of *hDIO1* mRNA. In contrast, overexpression of USF1/2 increased *hDIO1* promoter activity. Short interfering RNA-mediated knockdown of FOXA1 decreased the expression of *hDIO1* mRNA, but knockdown of both FOXA1 and FOXA2 restored it. The response of the *hDIO1* promoter to USF was greatly attenuated in the absence of FOXA1. Taken together, these results indicate that a balance of FOXA1 and FOXA2 expression modulates *hDIO1* expression in the liver. **(*Endocrinology* 153: 492–500, 2012)**

Thyroid hormone activation and inactivation are mediated by three selenoenzymes, type 1 iodothyronine deiodinase (D1), D2, and D3. D1 and D2 catalyze the conversion of $T_4$ to $T_3$ via removal of outerring iodine (1). The human D1 gene (*hDIO1*) is expressed in the liver, kidney, thyroid, and pituitary (2). The D2 gene is expressed in the central nervous system, pituitary, heart, and skeletal muscle, but it is absent in the liver (1). The D3 gene is expressed in the central nervous system and placenta, and it is involved in thyroid hormone inactivation by mediating the removal of innerring iodine. Unlike D2, D1 activity is considered to be regulated predominantly at the pretranslational level. The expression and activity of D1 are modulated by a variety of factors. $T_3$ induces the expression of *hDIO1* via two thyroid hormone responsive elements within its promoter (3), and nuclear factor κB induced by TNFα inhibits the $T_3$-dependent induction of D1 (4). However, the precise mechanism of the transcriptional regulation of *hDIO1* expression remains unclear.

In this study, we sought to identify factors that increased D1 activity in the liver, a main organ that expresses *hDIO1*. We assessed the promoter activity of the 5-kb 5′-flanking region of *hDIO1* and characterized regulatory element-binding proteins within this region. In this study, we identify responsive elements for the forkhead box (FOX) transcription factors FOXA1/FOXA2 and the ba-

ISSN Print 0013-7227 ISSN Online 1945-7170
Printed in U.S.A.

doi: 10.1210/en.2011-1310 Received May 30, 2011. Accepted October 17, 2011.
First Published Online November 8, 2011

Abbreviations: D1, Type 1 iodothyronine deiodinase; FOX, forkhead box; *hDIO1*, human D1 gene; HNF, hepatocyte nuclear factor; MUT, mutated oligonucleotide; siRNA, short interfering RNA; USF, upstream stimulatory factor; WT, wild type.

sic/helix-loop-helix-leucine zipper transcription factor upstream stimulatory factor (USF), and we show that FOXA1, FOXA2, and USF all participate in the regulation of *hDIO1*. We also show that FOXA1 is required for the activation of the *hDIO1* promoter by USF and that FOXA2 represses the transcription of *hDIO1* and disrupts the interaction of USF with FOXA1 by occupying the FOXA binding site. Collectively, these results demonstrate that FOXA1 and FOXA2 display opposing activity in the regulation of *hDIO1* expression in the liver.

## Materials and Methods

### Cell culture

The human liver carcinoma cell line HepG2 was obtained from American Type Culture Collection (Manassas, VA) and cultured in MEM (Life Technologies, Carlsbad, CA) with 0.1 mM nonessential amino acid solution (Life Technologies), 1 mM sodium pyruvate (Life Technologies), 100 U/ml penicillin, 100 μg/ml streptomycin, and 0.25 μg/ml amphotericin B supplemented with 10% fetal bovine serum (Sigma-Aldrich, St. Louis, MO) at 37 C in a humidified atmosphere containing 5% $CO_2$. TSA 201 cells, a clone of human embryonic kidney 293 cells (*5*), were cultured in DMEM (Life Technologies) with 100 U/ml penicillin, 100 μg/ml streptomycin, and 0.25 μg/ml amphotericin B supplemented with 10% fetal bovine serum at 37 C in a humidified atmosphere containing 5% $CO_2$.

### Plasmid construction

Deletion mutants of the 5′-flanking regions of *hDIO1* (−4949, −2023, −343, −187, −150, −131, and −103/−4, the translational start site was set at +1) were prepared by PCR using human genomic DNA from leukocytes as a template. The resulting PCR products were subcloned into *Eco*RV or *Kpn*I/*Hin*dIII-digested pGL4.10 (Promega, Madison, WI) to create a fusion with the luciferase gene (−4949, −2023, −343, −187, −150, −131, and −103/−4 hDIO1-Luc). The PCR primers, containing *Eco*RV, *Kpn*I, or *Hin*dIII linker, are listed in Table 1. The correct orientation of these deletion mutant constructs was confirmed by sequencing.

Mutations were created using the QuikChange Site-Directed Mutagenesis kit (Stratagene, La Jolla, CA), according to the manufacturer's instruction; −187/−4 and −150/−4 hDIO1-Luc were used as templates. For mutagenesis, the sequences of the FOXA binding element and E-box were specified in figure 3 below. Mutated constructs were isolated from each reaction and verified by sequencing.

Plasmids expressing cDNA for FOXA2 and USF1, pF1KB7038 and pF1KB8339, respectively, were generated by Kazusa DNA Research Institute (Chiba, Japan) and purchased from Promega. These plasmids were digested with *Sgf*I and *Pme*I, and cDNA for FOXA2 and USF1 were ligated into the *Sgf*I/*Pme*I-digested pF4A CMV Flexi vector (Promega), which uses the human cytomegalovirus intermediate-early enhancer/promoter to allow constitutive protein expression at native levels in mammalian cells. The open reading frame of human USF2 was generated by PCR using HeLa cell cDNA as a template. The PCR primers containing *Sgf*I or *Pme*I linker are listed in Table 1. The PCR product was digested with *Sgf*I and *Pme*I, cloned into the *Sgf*I/*Pme*I-digested pF4A CMV Flexi vector, and verified by sequencing.

### Transient transfection and luciferase assay

HepG2 and TSA 201 cells were plated at 1.5–2 × $10^5$ and 0.5–1 × $10^5$ cells/well in 24-well tissue culture plates, respectively. Cells were maintained in 0.5 ml of antibiotic-free medium for 1 d before transfection. Transient transfections were performed using the Lipofectamine LTX reagent (Life Technologies) for HepG2 cells and the Lipofectamine 2000 reagent (Life Technologies) for TSA 201 cells according to the manufacturer's instruction. In HepG2 cells, transfections included 500 ng of experimental reporter constructs and 25 ng of pGL4.74, which contained the cDNA encoding *Renilla* luciferase (Promega) as an internal control for transfection efficiency. In TSA 201 cells, transfections included 100 ng of experimental reporter constructs and 5 ng of pGL4.74. In the experiments with plasmids expressing FOXA2 and/or USF, total amount of plasmid DNA was kept constant by adding the corresponding amount of pF4A without a cDNA insert. After transfection, cells were grown in antibiotic-free medium and harvested after 48 h. Luciferase activity was determined using the Dual-Luciferase Reporter Assay System (Promega), and luminescence was measured by a 2030 ARVOX multilabel reader (PerkinElmer, Waltham, MA). Firefly luciferase activity was normalized to *Renilla* luciferase activity in each well to control for transfection efficiency.

### Computational analysis of the putative transcription factor binding sites

The putative transcription factor binding sites on the 5′-flanking region of *hDIO1* were identified by computational

**TABLE 1.** Oligonucleotides used in plasmid construction and RT-PCR

| | Forward primer (5′-3′) | Reverse primer (5′-3′) | Accession no. |
|---|---|---|---|
| Plusmid construction | | | |
| −4949/−4 hdio1-Luc | GGGGATATCGCAGGTGCAGCCTAGAGATGTAACG | CCCAAGCTTGGCAAAGCCAGAGTAAGCTC | AL031427 |
| −2023/−4 hdio1-Luc | CGGGGTACCACACTTCCATTCCAGTTACAG | CCCAAGCTTGGCAAAGCCAGAGTAAGCTC | AL031427 |
| −343/−4 hdio1-Luc | CGGGGTACCGAGAGAGCATCTAACAGGTTC | CCCAAGCTTGGCAAAGCCAGAGTAAGCTC | AL031427 |
| −187/−4 hdio1-Luc | CGGGGTACCGACCTTTGTGCACCTGGTTAG | CCCAAGCTTGGCAAAGCCAGAGTAAGCTC | AL031427 |
| −150/−4 hdio1-Luc | CGGGGTACCGACAGAAAGGCAAACATCTTC | CCCAAGCTTGGCAAAGCCAGAGTAAGCTC | AL031427 |
| −131/−4 hdio1-Luc | CGGGGTACCTCTGACCTGACTCCTTCCCCTG | CCCAAGCTTGGCAAAGCCAGAGTAAGCTC | AL031427 |
| −103/−4 hdio1-Luc | CGGGGTACCGGTTGGCTGCTCCTACCCTGC | CCCAAGCTTGGCAAAGCCAGAGTAAGCTC | AL031427 |
| pF4A-USF2 | AGCAGCGATCGCCATGGACATGCTGGACCCGGGTCTGGA | CGAGGTTTAAACCTGCCGGGTGCCCTCGCCCA | NM_003367 |
| RT-PCR | | | |
| hDIO1 | CAGAGTCAAGCGGAACATCC | CCGTTGGTCACCTAGAATTG | NM_000792 |
| Cyclophilin A | GCACTGGAGAGAAAGGATTTGG | CAGCAATGGTGATCTTCTTGC | NM_021130 |

analysis using TFSEARCH databases (http://www.cbrc.jp/research/db/TFSEARCHJ.html), based on the TRANSFAC databases (6).

### RNA isolation, RT-PCR, and quantitative PCR

Total RNA was extracted from HepG2 cells using the RNeasy Plus Mini kit (QIAGEN, Valencia, CA) according to the manufacturer's instruction. One microgram of total RNA was reverse transcribed with random hexamers using a First-strand cDNA Synthesis kit (GE Healthcare UK Ltd., Buckinghamshire, UK) according to the manufacturer's instruction. The resulting cDNA were diluted 1:10 and subjected to PCR amplification with 0.5 mM each of the sense and antisense primers and 0.5 U of AmpliTaq Gold DNA polymerase (Life Technologies). The PCR primers used for *hDIO1* and human cyclophilin A gene are indicated in Table 1. The PCR conditions were 40 cycles of denaturation for 1 min at 95 C, annealing for 1 min at 52 C, and extension for 1 min at 72 C. The PCR products were electrophoresed in 2% agarose gels.

Quantitative PCR reactions were performed, recorded, and analyzed using TaqMan Gene Expression Assays with StepOnePlus real-time PCR system (Life Technologies). The probe and primers were Hs00270129_m1 (human *FOXA1*), Hs00232764_m1 (human *FOXA2*), and Hs00174944_m1 (*hDIO1*) and purchased from Life Technologies. Diluted cDNA were amplified using the following conditions: 50 C for 2 min, 95 C for 10 min, and 40 cycles of 95 C for 15 sec and 60 C for 1 min, followed by continuous incubation at 25 C. Expression levels of FOXA1, FOXA2, and hDIO1 were normalized to cyclophilin A to compensate for variations in input RNA.

### Preparation of cell extracts and EMSA

Nuclear extracts were prepared from HepG2 cells using the Nuclear Extract kit (Active Motif, Carlsbad, CA), according to the manufacturer's instruction. EMSA were conducted using a LightShift chemiluminescent EMSA kit (Thermo Fisher Scientific, Rockford, IL) with slight modifications of the original manufacturer's instruction. Oligonucleotides 3′-end labeled with biotin were synthesized (Life Technologies) and annealed to generate double-stranded oligonucleotide probes. Two hundred femtomoles of oligonucleotide probe were incubated with 10–15 μg of nuclear protein and 0.5 μg of poly (dI-dC) in the presence or absence of competing oligonucleotide in 10× binding buffer [containing 100 mM Tris, 500 mM KCl, and 10 mM dithiothreitol (pH 7.5)] and 75 mM KCl, and 5% glycerol was added to solutions containing probes with an E-box element. After a 30-min incubation at room temperature, DNA-protein complexes were separated by electrophoresis on a 6% DNA retardation gel (Life Technologies) at 4 C in 0.5× Tris-borate, EDTA buffer [containing 89 mM Tris-borate and 2 mM EDTA (pH 8.0)]. For supershift assays, binding reactions were incubated for 45 min at room temperature with antibodies before the addition of labeled probes. The antibodies used in the supershift assays were as follows: 1 μl (200 μg/0.1 ml) of USF1 (sc-8983X), USF2 (sc-861X), E47 (sc-763X), FOXA1 (sc-6553X), FOXA2 (sc-6554X), and FOXA3 (sc-5361X) and 5 μl (200 μg/0.5 ml) of normal goat and normal rabbit IgG, and all were purchased from Santa Cruz Biotechnology, Inc. (Santa Cruz, CA). After electrophoresis, samples were transferred onto nylon membranes and fixed by UV irradiation. Biotinylated DNA was detected using a Fujix Lumino-image analyzer (LAS-1000; Fuji Photo Film Co., Ltd., Tokyo, Japan).

### Transfection of short interfering RNA (siRNA)

An aliquot of 6 pmol siRNA specific for FOXA1 and/or FOXA2 (Stealth Select RNAi, Life Technologies) or a negative control siRNA (Stealth RNAi Negative Control, Life Technologies) was transfected into HepG2 cells using the Lipofectamine RNAiMax reagent (Life Technologies) by reverse transfection according to the manufacturer's instruction. After transfection, HepG2 cells were plated at 1.5–2 × $10^5$ cells/well in 24-well tissue culture plates and maintained in 0.5 ml of antibiotic-free medium for 24–48 h. mRNA extraction and analysis were performed as described above.

### Statistics

The data represent the mean ± SEM and were obtained from at least three separate experiments, each performed in triplicate. Statistical analyses were performed to examine the significance of differences among the results using unpaired *t* test or ANOVA followed by Student-Newman-Keuls test or Dunnett's test.

## Results

### Functional analysis of the 5′-flanking region of the *hDIO1* gene

To identify regions within the promoter region of *hDIO1* important for regulating its expression, a series of 5′-deletion constructs was subcloned into the pGL4.10 vector and transiently transfected into HepG2 and TSA 201 cells (Fig. 1A). In both HepG2 and TSA 201 cells, luciferase activity increased by deletion of nucleotides −150 to −131 and decreased after deletion of −131 to −103. Among the tested constructs, the luciferase activity produced by transfection of −150/−4 hDIO1-Luc was specifically and markedly decreased in HepG2 cells. Additionally, more pronounced differences were seen between the activity of −150/−4 hDIO1-Luc and −131/−4 hDIO1-Luc in HepG2 cells compared with TSA 201 cells. In addition, luciferase activity was markedly increased by deleting the region from −343 to −187 and decreased after deletion of −187 to −150 only in HepG2 cells. Taken together, these results indicate that the region between nucleotides −187 and −132 is important for *hDIO1* promoter function in HepG2 cells. To confirm the expression of *hDIO1*, we performed RT-PCR using total RNA isolated from HepG2 and TSA 201 cells, a liver and kidney cell line, respectively. As shown in Fig. 1B, although there was a difference in the degree of gene expression, *hDIO1* was expressed in both cell lines; this was consistent with a previous report examining *hDIO1* tissue distribution (2). Additionally, multiple PCR products were detected, because there are several alternative splice variants of *hDIO1* (7). These results indicate that there may exist a sequence

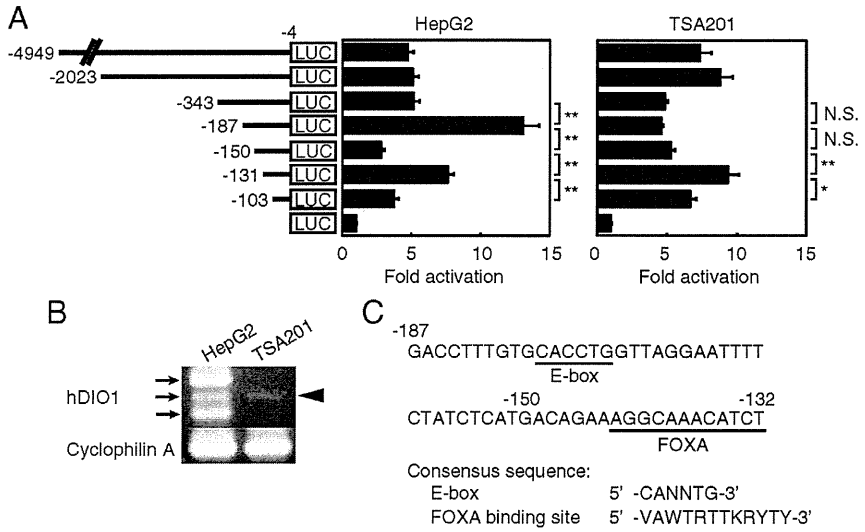


**FIG. 1.** Liver-specific changes in *hDIO1* promoter activity. A, A series of 5′-deletion constructs of the *hDIO1* promoter were transiently transfected into HepG2 or TSA 201 cells. Promoter activity was normalized to *Renilla* luciferase activity and expressed as the relative activity to promoterless pGL4.10. Statistical significance was determined by ANOVA followed by Student-Newman-Keuls test. *, $P < 0.05$; **, $P < 0.01$. N.S., Not significant. B, RT-PCR analysis of *hDIO1* expression. Electrophoretic analysis of RT-PCR products using total RNA from HepG2 and TSA 201 cells was performed. The *arrows* and *arrowhead* correspond to the RT-PCR products using total RNA from HepG2 and TSA 201 cells, respectively. Cyclophilin A was used as a positive control. C, The nucleotide sequences of the 5′-flanking region of *hDIO1* are shown. The translational start site was set at +1. *Underlined sequences* indicate putative binding sites for transcription factors. Consensus sequences of E-box site and FOXA binding site are shown at the *bottom*. Abbreviations for nucleotides: W (A or T), K (G or T), Y (C or T), R (A or G), V (A, C, or G), and N (A, C, G, or T). LUC, Luciferase.

essential for liver-specific expression of *hDIO1* within the −187 to −132 region of its promoter. A computational analysis of this region revealed the presence of a consensus E-box site between nucleotides −187 and −151 and a FOXA binding site between nucleotides −150 and −132 (Fig. 1C).

## Promoter activity associated with the FOXA binding site and the E-box

To better understand the contribution of the FOXA binding site and the E-box on the expression of *hDIO1* in liver-derived HepG2 cells, we examined luciferase activity in cells transfected with wild-type (WT) or mutated *hDIO1* promoter constructs. In HepG2 cells, luciferase activity was increased 2-fold by mutating the FOXA binding site when cells were transfected with a −150/−4 hDIO1-Luc construct (Fig. 2A). In addition, when cells were transfected with a −187/−4 hDIO1-Luc construct, luciferase activity was nearly completely lost by destruction of the E-box, and mutation of the FOXA binding site caused a decrease in luciferase activity by 50% (Fig. 2B). In TSA 201 cells transfected with −187/−4 hDIO1-Luc, luciferase activity was almost completely abolished by mutation of the E-box, but mutation of the FOXA binding site in both −187/−4 hDIO1-Luc and −150/−4 hDIO1-Luc did not significantly affect luciferase activity (Fig. 2). Thus, the E-box present within the *hDIO1* promoter is required for the enhancer activity in both liver- and kidney-derived cells, but the FOXA binding site exhibits liver-specific enhancer and repressor activity.

## Binding of FOXA1/FOXA2 to the FOXA binding site and USF to the E-box

To determine the transcription factors that bind to these elements in the promoter of *hDIO1* in HepG2 cells, we performed EMSA using oligonucleotides with the FOXA binding site and the E-box. Incubation of HepG2 cell extracts with oligonucleotides containing the FOXA binding site (Fig. 3A, WT-F) led to the formation of several DNA/protein complexes (Fig. 3B, lane 2). Formation of one of these complexes was inhibited by incubation with excess WT-F, but not mutated oligonucleotide (MUT)-F, demonstrating the specificity of this complex (Fig. 3B, lanes 3–6). Additionally, the complex was supershifted by addition of anti-FOXA1 and anti-FOXA2 antibodies (Fig. 3B, lanes 7 and 8). However, an antibody specific for FOXA3, which binds an identical sequence, or normal goat IgG did not disrupt complex formation (Fig. 3B, lanes 9 and 10). These results suggest that the putative FOXA binding site is specifically bound by FOXA1 or FOXA2. We next examined binding to the E-box sequence, and several complexes were formed by

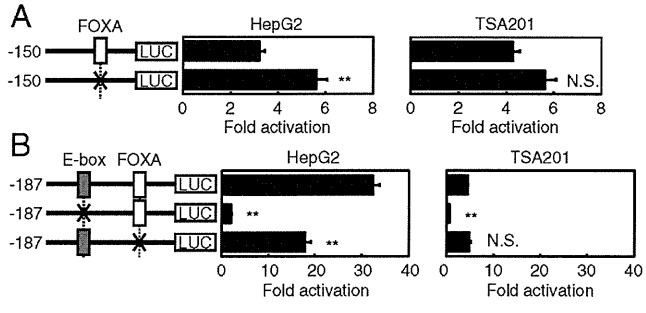


**FIG. 2.** Changes in *hDIO1* promoter activity by FOXA binding site and E-box. Schematic diagram in the *left* of each figure representing WT and site-specific mutations of the *hDIO1* promoter, introduced into the upstream region of the luciferase gene. A *cross* represents the site-specific mutation of the putative FOXA binding site or E-box. Each construct was transiently transfected into HepG2 or TSA 201 cells. Promoter activity was normalized to *Renilla* luciferase activity and expressed as the relative activity to promoterless pGL4.10. Statistical significance was determined by unpaired *t* test (A) or ANOVA followed by Dunnett's test (B). **, $P < 0.01$. N.S., Not significant.

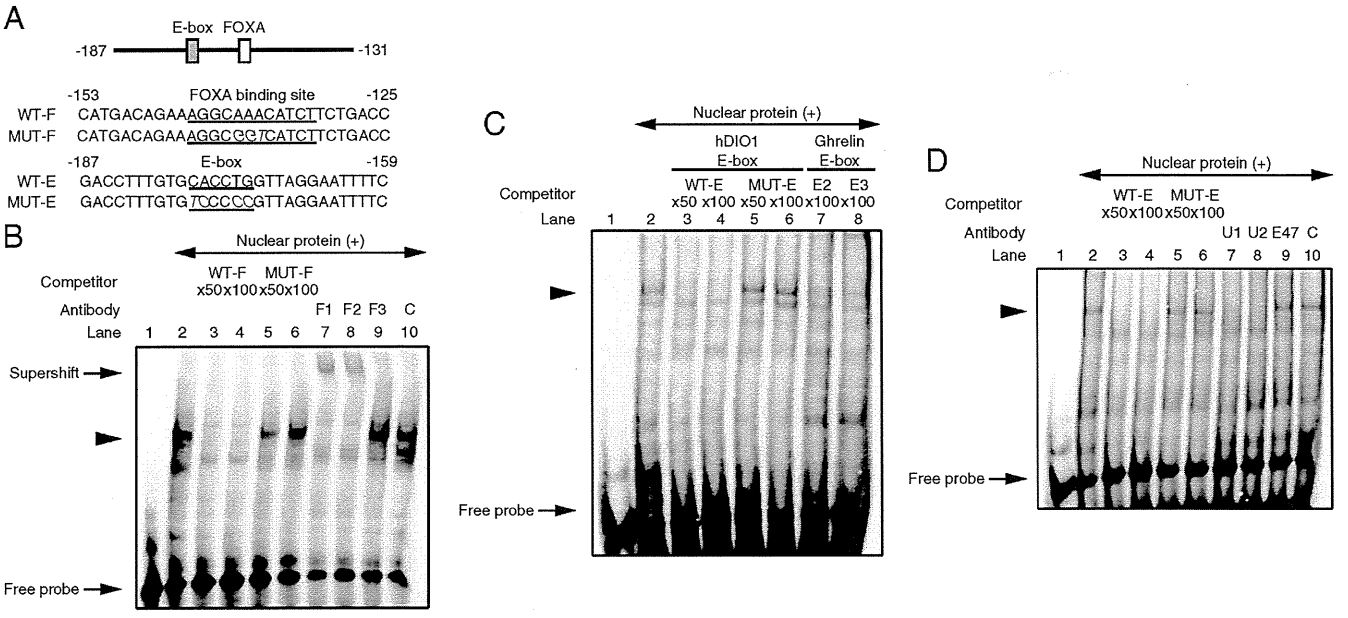


**FIG. 3.** Specific binding of the transcription factors within the −187 and −132 region in the *hDIO1* promoter using nuclear proteins from HepG2 cells. Panel A, Sequences of the double-stranded oligonucleotides used in EMSA. WT-F, WT *hDIO1* sequence identical to the −153 to −125 region, containing the FOXA binding site at −143 to −132. MUT-F contains a mutated FOXA binding site. WT-E, WT *hDIO1* sequence identical to the −187 to −159 region, containing the E-box at −177 to −172. MUT-E contains a mutated E-box. Each putative binding site is *underlined*; the mutated base pairs are indicated by *italic letters*. Panel B, Oligonucleotide WT-F was used as the probe for EMSA either without competitor (lane 2) or in the presence of 50- and 100-fold molar excesses of unlabeled WT-F (lanes 3 and 4, respectively) or MUT-F (lanes 5 and 6, respectively). The specific complex formed from HepG2 cell nuclear extract and WT-F is indicated by an *arrowhead*. Supershift assay experiments were performed using antibody against FOXA1 (F1; lane 7), FOXA2 (F2; lane 8), or FOXA3 (F3; lane 9) and normal goat IgG (C; lane 10). Panel C, Oligonucleotide WT-E was used as the probe for EMSA either without competitor (lane 2) or in the presence of 50- and 100-fold molar excesses of unlabeled WT-E (lanes 3 and 4, respectively), MUT-E (lanes 5 and 6, respectively), or 100-fold molar excesses of unlabeled E-box from the human ghrelin gene [E2 and E3 (in Ref. 8); lanes 7 and 8, respectively]. The specific complex formed from HepG2 cell nuclear extract and WT-E is indicated by an *arrowhead*. D, Supershift assay experiments were performed using antibody against USF1 (U1; lane 7), USF2 (U2; lane 8), or E47 (E47; lane 9) and normal rabbit IgG (C; lane 10). C, Negative control (normal goat and normal rabbit IgG).

incubation of HepG2 cell extracts with an appropriate oligonucleotide (Fig. 3A, WT-E, and C, lane 2). Formation of one of these complexes was inhibited by incubating with an excess of WT-E and the E-box from human ghrelin gene (8) but not by a mutant oligonucleotide MUT-E (Fig. 3C, lanes 3–8). Computational analysis predicted that the putative E-box site binds the basic/helix-loop-helix-leucine zipper transcription factor USF, and to investigate this hypothesis, a supershift assay was performed using antibodies specific for USF1 and USF2. Addition of antibodies specific for USF1 and USF2 completely inhibited complex formation (Fig. 3D, lanes 7 and 8). However, incubation with an antibody against E47, a protein that binds a similar E-box sequence, or normal rabbit IgG did not disrupt complex formation (Fig. 3D, lanes 9 and 10). These results suggest that USF1/USF2 bind the putative E-box, and this complex likely contains a USF1/USF2 heterodimer. Collectively, FOXA1, FOXA2, and USF likely participate in the regulation of *hDIO1* expression.

## Effect of overexpression of FOXA2 or USF on *hDIO1* promoter activity

To determine whether FOXA and USF have the potential to affect the activity of the *hDIO1* promoter in liver cells, a −187/−4 hDIO1-Luc construct was transiently transfected into HepG2 cells along with increasing amounts of either a FOXA2 or USF expression plasmid. The luciferase activity decreased in a dose-dependent manner by cotransfection of the FOXA2 expression plasmid with −187/−4 hDIO1-Luc (Fig. 4A). In contrast, luciferase activity increased dose dependently by the cotransfection of the USF1 or USF2 expression plasmid, and overexpression of USF2 consistently led to greater *hDIO1* promoter activity than expression of USF1 alone (Fig. 4B). Thus, transcription of *hDIO1* is negatively regulated by FOXA2 and positively regulated by USF. Although we transiently transfected a −187/−4 hDIO1-Luc construct into HepG2 cells along with increasing amounts of a FOXA1 expression plasmid, we could not obtain appropriate data, indicating that the FOXA1 expression plasmid we used did not function in our experimental system for unknown reason.

## RNA interference

Next, we determined the effects of FOXA on the native *hDIO1* promoter using siRNA-mediated knockdown of FOXA in HepG2 cells. As shown in Fig. 5, A and B, knock-